Invited Speaker

1186 Geological Materials and Bio-mineral systems
Dr David McNamara

Oral Presentation

348 Impact of physical exercise in bone healing around bio-resorbable implants imaged by synchrotron techniques
Irene Rodriguez Fernandez[1], Thomas Bretschneider[2], Omer Suljevic[3], Annelie Weinberg[3], Nicole Sommer[3], Goran Lovric[1], Tilman Grunewald[4,5], Helga Lichtenegger[2], Andreas Menzel[1]
[1]Photon Science Division, Paul Scherrer Institut, 5232 Villigen PSI, Switzerland, [2]Institute of Physics and Materials Science, University of Natural Resources and Life Science (BOKU), 1190 Vienna, Austria, [3]Department of Orthopedics and Traumatology, Medical University of Graz, 8036 Graz, Austria, [4]Aix-Marseille Univ, CNRS, Centrale Marseille, Institut Fresnel, 13013 Marseille, France, [5]The European Synchrotron, Avenue des Martyrs 71, 38000 Grenoble, France
470 Additive effects in phase transformation of calcium phosphate to hydroxyapatite using high-throughput transmission electron microscopy
Miss Johanna Neumann Sørensen[1], Assistant Professor Murat Nulati Yesibolati[1]
[1]Technical University of Denmark (DTU), kgs. lyngby, Denmark
523 Functional chemistry of minimally altered organic matter in the meteorite Winchcombe probed by monochromated EELS
Dr Aleksander Buseth Mosberg[1], Dr Christian Vollmer[2], Dr Demie Kepaptsoglou[1,3], Dr Jan Leitner[4,5], Dr Khalil El Hajraoui[1], Dr Ashley J. King[6], Ms. Charlotte L. Bays[6,7], Dr Paul F. Schofield[6], Dr Tohru Araki[8,9], Prof. Quentin M. Ramasse[1,10]
[1]SuperSTEM Laboratory, SciTech Daresbury, Daresbury, UK, [2]Institut für Mineralogie, University of Münster, Münster, Germany, [3]School of Physics, Engineering and Technology, University of York, Heslington, UK, [4]Institut für Geowissenschaften, Ruprecht-Karls-Universität Heidelberg, Heidelberg, Germany, [5]Max Planck Institute for Chemistry, Particle Chemistry Department, Mainz, Germany, [6]Planetary Materials Group, Natural History Museum, , UK, [7]Department of Earth Sciences, Royal Holloway, University of London, Egham, UK, [8]Diamond Light Source, Harwell Science and Innovation Campus, Didcot, UK, [9]National Institutes of Natural Sciences, Institute for Molecular Science, UVSOR Synchrotron Facility, Okazaki, Japan, [10]School of Chemical and Process Engineering and School of Physics and Astronomy, University of Leeds, Leeds, UK
1008 2D and 3D EELS Analyses on the Low-Energy Core-Loss Edges in Beam-sensitive Ryugu Asteroid Samples
Dr Mario Pelaez-Fernandez[1,2,3], Dr Maya Marinova[4], Dr Adrien Teurtrie[1], Dr Simon Hettler[1], Sylvain Laforet[1], Dr Corentin Le Guillou[1], Prof. Hugues Leroux[1], Dr Raul Arenal[2,3], Dr Francisco De la Peña[1]
[1]Unité Matériaux et Transformations (UMET UMR 8207), Université de Lille, Bâtiment C6, Cité Scientifique, Villeneuve d'Ascq, France, [2]Instituto de Nanociencia y Materiales de Aragon (INMA), CSIC-U. de Zaragoza, Zaragoza, Spain, [3]Laboratorio de Microscopias Avanzadas, Universidad de Zaragoza, Zaragoza, Spain, [4]Univ. Lille, FR 2638-IMEC-Institut Michel-Eugène Chevreul, Lille, France
1051 Multiscale 3D organization of human auditory ossicles unveiled by synchrotron small-angle X-ray scattering tensor tomography
Dr Margaux Schmeltz[1], Dr Christian Appel[1], Ginevra Lautizi[2], Irene Rodriguez Fernandez[1], Torne Tänzer[1], Prof. Dr. Med. Lukas Anschuetz[3,4], Dr Meitian Wang[1], Prof. Dr. Marianne Liebi[1,5,6]
[1]Paul Scherrer Institute, Swiss Light Source, Villigen, Switzerland, [2]Department of Physics, University of Trieste, Trieste, Italy, [3]Otorhinolaryngology Dept., Head and Neck Surgery, Inselspital University Hospital, Bern, Switzerland, [4]Hearing Research Laboratory, ARTORG Center, University of Bern, Bern,

Switzerland, [5]Department of Physics, Chalmers University of Technology, Gothenburg, Sweden, [6]Institute of Materials, Ecole Polytechnique Fédérale de Lausanne (EPFL), Lausanne, Switzerland

Poster Presentation

78 Deep learning 3D-mineral liberation analysis with micro-X-ray fluorescence, micro-computed tomography, and deep learning segmentation
Dr. Patrick Tung[1,2], Amalia Halim[1], Dr. Helen Wang[1], Dr. Anne Rich[1], Dr. Xiao Chen[3], Prof. Klaus Regenauer-Lieb[4], Dr. Christopher Marjo[1]
[1]Mark Wainwright Analytical Centre (MWAC), University of New South Wales, UNSW Sydney, Australia, [2]Research Technology Services, University of New South Wales, UNSW Sydney, Australia, [3]Mineral Resources, Commonwealth Scientific and Industrial Research Organisation (CSIRO), Kensington, Australia, [4]WA School of Mines: Minerals, Energy and Chemical Engineering, Australian Resources Research Centre (ARRC), Curtin University, Kensington, Australia
193 Nanoscale arrangement of the healthy dentin and comparison with the dentino-genesis imperfecta-affected dentin
Dr Maxime Vallet[1,2], Dr Margot Riou[3], Mme Margot Leclercq[1], Dr Elsa Vennat[1]
[1]Université Paris-Saclay, CentraleSupélec, ENS Paris-Saclay, CNRS, LMPS, Gif-sur-Yvette, France , [2]Université Paris-Saclay, CentraleSupélec, CNRS, SPMS, Gif-sur-Yvette, France, [3]Universite de Paris, Dental Faculty, Paris, France
212 Electron microscopy characterization of king scallop (Pecten maximus) shells from low-voltage SEM to 3D-EBSD reconstruction
Dr Lise Guichaoua[1], Dr Benazir Khurshid[3], M Arnaud Benchetrite[3], Ms Stéphanie Bessette[1], Dr Bryce Stewart[2], Pr Natalie Reznikov[3], Pr Roland Kröger[4], Pr Raynald Gauvin[1]
[1]McGill Electron Microscopy Research Group, Department of Mining and Materials Engineering, McGill University , Montreal, Canada, [2]Marine Biological Association, Plymouth, United Kingdom, [3]Department of Bioengineering, Faculty of Engineering, McGill University, Montreal, Canada, [4]School of Physics, Engineering and Technology, University of York, York, United Kingdom
267 From Tarquinia's Necropolis to biorestoration: the role of the characterization in a multidisciplinary research context
Francesco Mura[1,2], Francesca Benedetti[3], Matilde Kratter[3], Luca Buccini[1], Pierfrancesco Atanasio[1], Anacleto Proietti[1], Angela Cirigliano[3], Daniele Passeri[1,2], Teresa Rinaldi[2,3], Marco Rossi[1,2]
[1]Department of Basic and Applied Sciences for Engineering (SBAI), Sapienza University of Rome, Rome, Italy, [2]CNIS-Center for Nanotechnology Applied to Industry of Sapienza, Sapienza University of Rome, Rome, Italy, [3]Department of Biology and Biotechnologies “Charles Darwin”, Sapienza University of Rome, Rome, Italy
388 Correlating absorption and diffraction contrast tomography on earth and space materials
Olivia Barbee[1], Jette Oddershede[1], Matthew Pankhurst[2], Florian Bachmann[1], Stephen Hall[3], Jonas Engqvist[3], Rhian Jones[4], Anders Svensson[5], Erik Lauridsen[1], Jun Sun[1]
[1]Xnovo Technology ApS, Køge, Denmark, [2]ITER/INVOLCAN, Tenerife, Spain, [3]Lund University, Lund, Sweden, [4]The University of Manchester, Manchester, UK, [5]University of Copenhagen, Copenhagen, Denmark
563 Carbonaceous inclusions from the oldest sediments on Earth
Magnus Harding[1,2], Austin Jarl Boyd[1], Sandra Siljeström[3], Madina Shamsuyeva[4], Pooyan Aliuos[4], Minik Rosing[1], Tue Hassenkam[1]
[1]Globe Institute, University of Copenhagen, Copenhagen, Denmark, [2]Sino-Danish College (SDC), University of Chinese Academy of Sciences, Beijing, China, [3]RISE Research Institutes of Sweden, Stockholm, Sweden, [4]Institute of Plastics and Circular Economy IKK, Leibniz University Hannover, Hannover, Germany

841 The EXCITE² Network: a European infrastructure providing transnational access to leading-edge imaging facilities
Alireza Chogani[1], Oliver Plümper[1], Geertje ter Maat[1], the EXCITE team
[1]Department of Earth Sciences, Utrecht University, Utrecht, The Netherlands
844 Thallium and arsenic incorporation in roméite group minerals
Priv.-Doz. Dr. Tamara Đorđević[1,2], Priv.-Doz. Dr. Michael Stöger-Pollach[1], Dr. Sabine Schwarz[1]
[1]E057-02 USTEM, Vienna University of Technology, Vienna, Austria, [2]Department of Mineralogy and Crystallography, University of Vienna, Vienna, Austria
886 Biorestoration Potential of Carbonatogenic Bacteria on Lithotypes: SEM and AFM characterization
Dr. Luca Buccini[1], Francesca Benedetti[2], Matilde Kratter[2], Francesco Mura[1,3], Anacleto Proietti[1], Pierfrancesco Atanasio[1], Angela Cirigliano[2], Marco Rossi[1,3], Teresa Rinaldi[1,2], Daniele Passeri[1,3]
[1]Department of Basic and Applied Sciences for Engineering (SBAI), La Sapienza University of Rome, Rome , Italy, [2]Department of Biology and Biotechnologies “Charles Darwin”, Sapienza University of Rome, Rome, Italy, [3]CNIS-Center for Nanotechnology Applied to Industry of La Sapienza, La Sapienza University of Rome, Rome, Italy
1102 Room temperature viscoplastic response of amorphous olivine films revealed by ex/in-situ TEM nanomechanical testing
Dr Armand Béché[1]
[1]IMAP/LACaMi - UCLouvain, Louvain-La-Neuve, Belgium
1124 SEM Automated Quantitative Mineralogy Method-development with Mineralogic: 200-nm-resolution Quantitative Assessment and Mineral-specific element mapping
Phd Nynke Keulen[1], MSc Sebastian N. Malkki[1], PhD Rikke Weibel[1], PhD Adam Garde[1]
[1]GEUS: Geological Survey of Denmark and Greenland, Copenhagen,
1146 ESEM technique for monitoring the geo-polymerization mechanism of the wet ash-cement mixture
Phd Bogdan Stefan Vasile[1], Dr. Iulian Boerasu[3], Dr. Adrian-Vasile Surdu[2], Dr. Adrian Ionut Nicoara[2]
[1]Research Center for Advanced Materials, Products and Processes, National University of Science and Technology POLITEHNICA Bucharest, 060042 Bucharest, Romania, Bucharest, Romania, [2]Department of Science and Engineering of Oxide Materials and Nanomaterials, Faculty of Applied Chemistry and Materials Science, University Politehnica of Bucharest, 011061 Bucharest, Romania, Bucharest, Romania, [3]National Research Center for Micro and Nanomaterials, Faculty of Applied Chemistry and Materials Science, University Politehnica of Bucharest, 060042 Bucharest, Romania, Bucharest, Romania

1186

Geological Materials and Bio-mineral systems

Dr David McNamara

PS-06, Lecture Theater 1, august 29, 2024, 10:30 - 12:30

348

Impact of physical exercise in bone healing around bio-resorbable implants imaged by synchrotron techniques

Irene Rodriguez Fernandez[1], Thomas Bretschneider[2], Omer Suljevic[3], Annelie Weinberg[3], Nicole Sommer[3], Goran Lovric[1], Tilman Grunewald[4,5], Helga Lichtenegger[2], Andreas Menzel[1]
[1]Photon Science Division, Paul Scherrer Institut, 5232 Villigen PSI, Switzerland, [2]Institute of Physics and Materials Science, University of Natural Resources and Life Science (BOKU), 1190 Vienna, Austria, [3]Department of Orthopedics and Traumatology, Medical University of Graz, 8036 Graz, Austria, [4]Aix-Marseille Univ, CNRS, Centrale Marseille, Institut Fresnel, 13013 Marseille, France, [5]The European Synchrotron, Avenue des Martyrs 71, 38000 Grenoble, France

PS-06, Lecture Theater 1, august 29, 2024, 10:30 - 12:30

Background incl. aims
Bio-resorbable magnesium implants are promising candidates for the treatment of bone fractures due to their mechanical properties, their immunological response during healing, and the reduced need to perform a second surgery for implant removal. Some studies show how the placement of bio-resorbable implants alters the bone nanostructure, which changes from the preferred orientation along the bone shaft to a wrapping around the implant surface [1].
There are, however, no accounts in the literature on how physical exercise applied immediately after implantation might influence the bone nanostructure and the healing process around magnesium implants. This question is of great importance for understanding the impact of mechanical stimuli during healing and could be of relevance for post-surgical recovery treatments.
Methods
We designed an animal study on two groups of rats, one group underwent physical exercise immediately after implantation and the other one was sedentary. The bone with the implant was explanted after 2 and 6 weeks and the explants were studied.
For the aims of the study, we used two complementary synchrotron 3D imaging techniques, i.e. small-angle scattering tensor tomography (SASTT) and phase-contrast high-resolution computed tomography (PCμCT). Each one of the samples was measured with both techniques and the results were correlated with each other.
Results
We have investigated the role physical exercise plays in bone healing around Mg implants in a short-term study. With SASTT we studied the orientations of the bone nanostructure in 3D [2]. We have observed how the degree of orientation of hydroxyapatite, the thickness of the mineral particles, and the nanostructural orientations in bone change when physical exercise is applied. With PCμCT we characterized the osteocytes' network (considered responsible for mechanotransduction) by imaging the lacunae in 3D. We performed a shape and orientation analysis of the osteocytes to study the effect that physical exercise has on this network, and we correlated the results of both techniques.
Conclusion
Our study proved that physical exercise favors remodeling and bone healing around bio-degradable implants and alters the orientation of the bone structures at different length scales. These results are highly relevant for understanding degradable implants' behavior and are expected to be of clinical significance in the treatment of bone fractures.

Keywords:

Bone, implants, physical exercise, X-ray

Reference:

[1] M. Liebi et al. (2021) 3D nanoscale analysis of bone healing around degrading Mg implants studied by X-ray scattering tensor tomography. Doi: 10.1101/2020.11.09.375253\
[2] Liebi, M. et al. Nanostructure surveys of macroscopic specimens by small-angle scattering tensor tomography. Nature 527, 349–352 (2015). https://doi.org/10.1038/nature16056

470

Additive effects in phase transformation of calcium phosphate to hydroxyapatite using high-throughput transmission electron microscopy

Miss Johanna Neumann Sørensen[1], Assistant Professor Murat Nulati Yesibolati[1]
[1]Technical University of Denmark (DTU), kgs. lyngby, Denmark

PS-06, Lecture Theater 1, august 29, 2024, 10:30 - 12:30

Background:
Calcium phosphate (CaP) is a crucial biomineral essential for human health, primarily forming the foundation of bones and teeth [1]. The nucleation of CaP begins from amorphous calcium phosphate (ACP) phases and transitions to hydroxyapatite (HAP), a key process in the mineralization of bones and teeth [2]. The mechanisms behind this phase transformation are complex and, despite decades of research, remain a topic of ongoing debate, particularly regarding the influence of additives such as Mg2+ [3]. This study aims to delve into the effects of Mg2+ on the transformation of ACP to HAP, employing high-throughput transmission electron microscopy (TEM) [4]for detailed analysis.

Methods:
To assess the impact of additives on phase transformation, we designed an automated sample preparation platform. This system uses a standard 24-well plate, complemented by a picoliter-volume liquid dispenser and a motorized stage under precise control. Custom Python scripts automate the liquid dispensing and stage movements, facilitating the accurate placement of 30 samples on a single TEM grid for comprehensive TEM analysis. Chemical reactions were initiated with three base solutions: 20 mM calcium chloride (CaCl2), 10 mM magnesium chloride (MgCl2), and 12 mM sodium phosphate (NaH2PO4). CaCl2 and MgCl2 solutions were mixed in various Mg2+/Ca2+ ratios (0, 0.01, 0.06, 0.3, and 0.5), as shown in Figure 1a. The addition of sodium phosphate solution and extra water marked the start of the reaction. Samples were extracted 3 minutes after the reaction's initiation, with a 300 pL aliquot deposited onto a TEM grid. This sampling continued at 45, 90, 135, 180, and 225-minute intervals on the same grid. Each 300 pL sample dried in about 2 seconds, creating distinct areas roughly 130 µm in diameter as in Figure 1a. The dispenser was cleaned after each sampling. Results were analyzed using bright-field TEM and electron diffraction, revealing insights into the samples' morphological and structure as illustrated in Figure 1.

Results:
Samples 1, 2, and 3 showed similar morphological evolutions: spheroidal nanoparticles formed within 3 minutes, transitioning into sheet-like nanostructures characteristic of HAP, as evidenced in Figures 1b and c. Diffraction patterns at 45 minutes confirmed the crystalline structure of HAP, indicating the shift from ACP to HAP. Mg2+ addition was found to expedite this crystallization, as seen in sample 3's radial average diffraction pattern, where HAP's distinctive peaks were more pronounced compared to samples 1 and 2. However, excessive Mg2+ concentrations delayed or prevented the ACP to HAP conversion, as demonstrated in Figures 1c and d, where sample 4 showed a delayed HAP transformation at 225 minutes, and notably, sample 5 did not transition to HAP even after 225 minutes.

Conclusion:
The innovative automated sample preparation platform significantly enhances our capacity to deposit multiple samples on a single TEM grid, enabling thorough investigation of the ACP to HAP phase transition with and without additives across various reaction times. This study highlights the advantages of applying high-throughput TEM for deep dives into chemical and biochemical reaction mechanisms. Our findings suggest that while Mg2+ does not affect the initial ACP formation, it does

modify the crystallization rate. Crystallization accelerates up to a Mg2+/Ca2+ ratio of 0.06, after which it slows down or stops the ACP to HAP conversion. Future work will aim to refine TEM techniques, such as optimizing sampling rates and integrating data acquisition processes, including in-situ methods like liquid-phase TEM [5], to further elucidate the mechanisms in-situ.

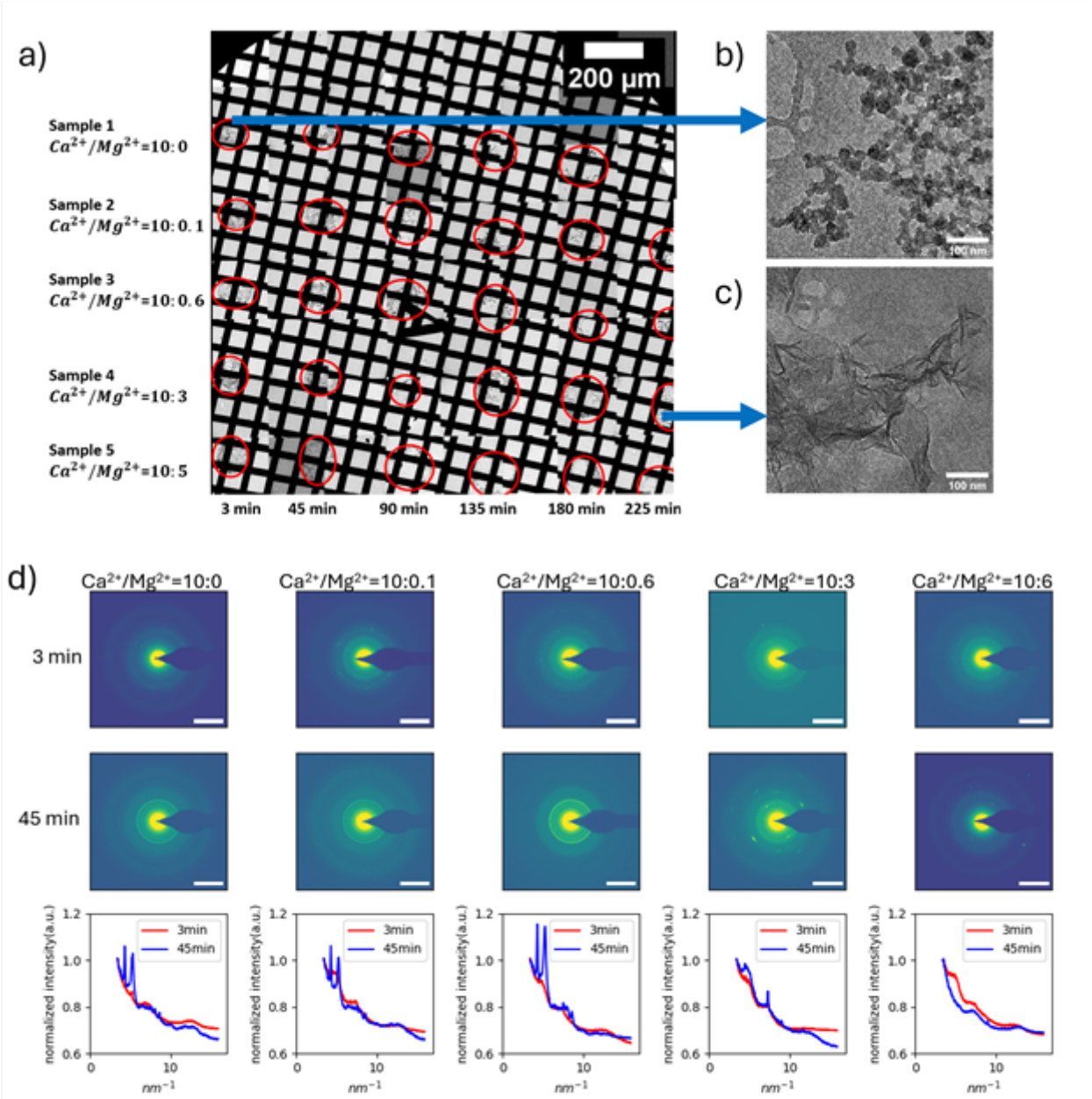

Figure 1. a) A bright-field transmission electron microscopy (BF-TEM) image capturing 30 distinct samples arranged on a single TEM grid via a custom-built sample preparation platform; b) Calcium phosphate (CaP) particles within the first sample observed post a 3-minute reaction interval; c) Hydroxyapatite within the fourth sample, after enduring a 225-minute reaction time; d) Expanded views of diffraction patterns alongside radial averages from the electron diffraction patterns across various samples, documented at different reaction times. The scale bar is 5 nm^{-1}

Keywords:

hydroxyapatite, additive, high-throughput TEM

Reference:

[1]S. V DorozhkinM. Epple, Biological and Medical Significance of Calcium Phosphates, Angewandte Chemie International Edition 41, 3130 (2002).
[2]H. Pan, X. Y. Liu, R. Tang, and H. Y. Xu, Mystery of the Transformation from Amorphous Calcium Phosphate to Hydroxyapatite, Chemical Communications 46, 7415 (2010).

[3]H. Ding, H. Pan, X. Xu, and R. Tang, Toward a Detailed Understanding of Magnesium Ions on Hydroxyapatite Crystallization Inhibition, Cryst Growth Des 14, 763 (2014).
[4]X. Gong, K. Gnanasekaran, K. Ma, C. J. Forman, X. Wang, S. Su, O. K. Farha, and N. C. Gianneschi, Rapid Generation of Metal–Organic Framework Phase Diagrams by High-Throughput Transmission Electron Microscopy, J Am Chem Soc 144, 6674 (2022).
[5]S. Canepa, M. N. Yesibolati, J. Schiøtz, S. Kadkhodazadeh, W. Huang, H. Sun, and K. Mølhave, Initiation and Progression of Anisotropic Galvanic Replacement Reactions in a Single Ag Nanowire: Implications for Nanostructure Synthesis, ACS Appl Nano Mater 4, 12346 (2021).

523

Functional chemistry of minimally altered organic matter in the meteorite Winchcombe probed by monochromated EELS

Dr Aleksander Buseth Mosberg[1], Dr Christian Vollmer[2], Dr Demie Kepaptsoglou[1,3], Dr Jan Leitner[4,5], Dr Khalil El Hajraoui[1], Dr Ashley J. King[6], Ms. Charlotte L. Bays[6,7], Dr Paul F. Schofield[6], Dr Tohru Araki[8,9], Prof. Quentin M. Ramasse[1,10]
[1]SuperSTEM Laboratory, SciTech Daresbury, Daresbury, UK, [2]Institut für Mineralogie, University of Münster, Münster, Germany, [3]School of Physics, Engineering and Technology, University of York, Heslington, UK, [4]Institut für Geowissenschaften, Ruprecht-Karls-Universität Heidelberg, Heidelberg, Germany, [5]Max Planck Institute for Chemistry, Particle Chemistry Department, Mainz, Germany, [6]Planetary Materials Group, Natural History Museum, , UK, [7]Department of Earth Sciences, Royal Holloway, University of London, Egham, UK, [8]Diamond Light Source, Harwell Science and Innovation Campus, Didcot, UK, [9]National Institutes of Natural Sciences, Institute for Molecular Science, UVSOR Synchrotron Facility, Okazaki, Japan, [10]School of Chemical and Process Engineering and School of Physics and Astronomy, University of Leeds, Leeds, UK

PS-06, Lecture Theater 1, august 29, 2024, 10:30 - 12:30

Background incl. aims
The composition of organic matter (OM) in meteorites such as carbonaceous chondrites is a useful indicator for the type of organic matter present on early, prebiotic earth [1]. This OM can be extracted with solvents and analysed with mass spectrometers, but these techniques lose local petrographic context, and the sometimes harsh chemical processes involved in the extraction have the potentially to unintentionally alter the detailed functional chemistry of the OM. Here, careful preparation of thin lamellas using focused ion beam (FIB) techniques, and correlative analysis by high-resolution electron energy loss spectroscopy (EELS) and scanning transmission x-ray microscopy (STXM) of the very same samples, allow for a detailed OM characterization at the nanoscale [2] within the OM's native petrographic context and with minimal alteration.

Methods
Using a Hitachi Ethos NX5000 triple-beam FIB system, several lamellas were prepared containing OM from the meteorite Winchcombe, with special care taken to minimize the impact from sample preparation and enable the study of minimally altered OM. Steps taken to minimize alteration include minimizing the use of protection layers where possible to avoid carbon contamination, backside milling to ensure FIB-deposited material is downstream of the thinned area, and rocking milling to improve uniformity. Where FIB deposition was necessary, metal-containing deposits only (Pt, W) were used, ensuring that any redeposition could be easily identified. Most lamellas were thinned to ≤ 40 nm, a thickness optimised both for sufficient EELS signal at low kV as well as for complementary STXM analysis of the same lamella. To minimize surface damage, crucial for thin samples, Ga+ milling was followed by 1 kV Ar+ polishing using the 'third beam' of the NX5000. Careful, targeted broad-beam low-energy Ar+ polishing, with repeated short exposures and multiple incident angles proved highly effective at reducing surface amorphization and Ga-implantation-related damage. The application of Ar+ polishing directly in the FIB offers here an additional degree of control during the final thinning procedure while minimizing sample handling, thus further lowering any risk of alteration to the OM. SEM imaging of thin areas was also limited and performed at low beam energies to mitigate electron beam alteration of the OM.
Monochromated EELS was carried out at 60 kV in a Nion UltraSTEM100MC-Hermes equipped with a Nion IRIS spectrometer and a DECTRIS ELA direct electron detector. With the samples in ultra-high vacuum, a probe size of 0.1 nm with low beam current of < 5pA, together with an energy resolution of 50-90 meV, makes it possible to distinguish local variations in the different bonds in carbon- and

nitrogen-containing OM. Both nanoglobules (~ 300 nm) and 'diffuse' carbon infiltrated into the phyllosilicate matrix (< 100 nm) were analysed. Complementary X-ray absorption near-edge structure (XANES) analysis in the STXM was carried out at the 108 beam-line of Diamond Light Source, UK with a nominal beam size of ~ 40 nm and energy step sizes of 0.1 to 0.5 eV. Where possible, both XANES and EELS were carried out on the same lamella, allowing for direct comparison and highlighting the complementarity of these related techniques.

Results

Both STXM-XANES and STEM-EELS reveal distinctive C K absorption bands at 285 and 286.5 eV across all lamellas, relating to aromatic carbon and aromatic ketone/aldehyde bonds. The superior spatial resolution of the STEM probe highlights local variations in the 285 eV aromaticity-linked peak, with a generally higher ratio of aromatic/aliphatic content compared to CM chondrites, indicative of higher alteration. The low noise of direct electron detector-based EELS also enables probing the functional chemistry of the less abundant nitrogen (atomic N/C ratios of only a few %). N K distinct bands are at 398.8 eV and 399.8 eV, associated with C-N double and triple bonds, respectively. Applying statistical denoising methods enables the detection of energy bands beyond those distinguishable in the STXM data, pointing to the presence in nanoscale areas of amino acids such as L-alanine, which had been previously detected by soluble OM studies [3]. Here, the variation of this 402-403 eV fine structure at small length scales, together with the care taken to provide as unaltered a view of the OM as possible within its petrographic context, suggest these functional groups can be linked unambiguously to fluid processes within the OM.

Conclusion

The combination of STXM-XANES and high-resolution STEM-EELS on carefully prepared, minimally altered FIB lamellas allows for the analysis of OM at the smallest length scales. Different nanoscale textures such as nanoglobules and diffuse OM can be distinguished and compared to learn about the evolution and alteration mechanics of organics in carbonaceous chondrites. The direct correlation and excellent match between STXM and 60 kV STEM-EELS results demonstrate how this approach provides a powerful characterization tool for complex extraterrestrial samples with a unique combination of high spatial and energy resolutions.

Figure: (a) scanning electron micrograph of an extracted FIB lamella. The top is thinned to electron transparency and exhibits both a bigger irregular OM grain and smaller patches of OM. (b-c) STEM-EELS + STXM data of the C-K and N-K edges. EELS – 1 and 2 correspond to regions indicated in (a). Subtle changes in the EELS spectrum can be observed for OM areas, even in close proximity.

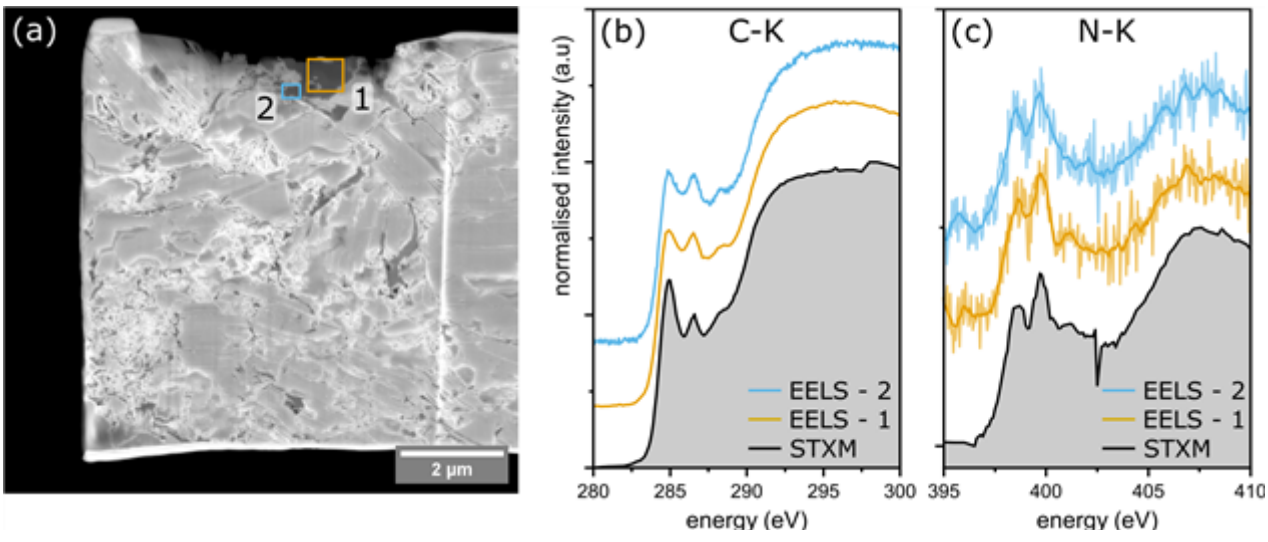

Keywords:

EELS, meteorite, Winchcombe, FIB

Reference:

[1] Vollmer, C., Kepaptsoglou, D., Leitner, J. et al. High-spatial resolution functional chemistry of nitrogen compounds in the observed UK meteorite fall Winchcombe. Nat Commun 15, 778 (2024). doi: 10.1038/s41467-024-45064-x
[2] Vollmer, C., Kepaptsoglou, D., Leitner, J. et al. Fluid-induced organic synthesis in the solar nebula recorded in extraterrestrial dust from meteorites. PNAS 111.43, 15338-15343 (2014). doi: 10.1073/pnas.1408206111
[3] Chan, Q. H. S., Watson, J. S., Sephton, M. A. et al. The amino acid and polycyclic aromatic hydrocarbon compositions of the promptly recovered CM2 Winchcombe carbonaceous chondrite. Meteor. Planetary Sci. 1-30 (2023). doi: 10.1111/maps.13936

1008

2D and 3D EELS Analyses on the Low-Energy Core-Loss Edges in Beam-sensitive Ryugu Asteroid Samples

Dr Mario Pelaez-Fernandez[1,2,3], Dr Maya Marinova[4], Dr Adrien Teurtrie[1], Dr Simon Hettler[1], Sylvain Laforet[1], Dr Corentin Le Guillou[1], Prof. Hugues Leroux[1], Dr Raul Arenal[2,3], Dr Francisco De la Peña[1]
[1]Unité Matériaux et Transformations (UMET UMR 8207), Université de Lille, Bâtiment C6, Cité Scientifique, Villeneuve d'Ascq, France, [2]Instituto de Nanociencia y Materiales de Aragon (INMA), CSIC-U. de Zaragoza, Zaragoza, Spain, [3]Laboratorio de Microscopias Avanzadas, Universidad de Zaragoza, Zaragoza, Spain, [4]Univ. Lille, FR 2638-IMEC-Institut Michel-Eugène Chevreul, Lille, France

PS-06, Lecture Theater 1, august 29, 2024, 10:30 - 12:30

Background

The Hayabusa2 space mission from the Japan Aerospace Exploration Agency returned materials from the Ryugu C-type asteroid to Earth in 2020. Due to its lack of atmosphere and low mass, Ryugu is less altered than other space bodies in the Solar System, preserving information about its primordial stages. One of its most interesting features is its phyllosilicate fibrous matrix, which can feature absorbed water and organic matter, as evidenced by remote infrared measurements[1] and laboratory analyses[2].

This matrix contains two families of phyllosilicates with different, albeit similar, chemical compositions and crystallographic structures: saponites (with a higher Si stoichiometry) and serpentines (with the presence of Al), intimately mixed at the nanoscale in a fibrous matrix and surrounded by various other systems such as sulfurs, and organic matter.

Until recently, the high sensitivity of the material to the electron beam[3] made it very difficult to perform electron microscopy analysis at the resolution required to address some intriguing questions, such as the presence of organic matter in the interlayers and the precise morphology of the intermixing of the different phyllosilicate families. Fortunately, the advent of direct electron detection, along with other instrumental and data analysis advances, has begun to expand the scope of analyses that can be performed in such beam-sensitive systems. Exciting recent developments include vibrational EELS[4] and 4D-STEM [5] analyses on Ryugu samples.

Here, we bring together several state-of-the-art techniques to achieve EELS analysis of FIB lamellas at unprecedented spatial resolution and EELS analytical tomography of nanopillars of these beam-sensitive samples. In particular, we utilize a hybrid-pixel direct electron detector for EELS acquisition, which offers almost perfect DQE, high-speed acquisition, and a wide dynamic range. This enables the development of a highly sensitive EELS analysis approach for all elements of interest in the sample. In particular, we acquire EELS low-loss spectrum images (SIs), instead of the usual core-loss and corresponding low-loss SIs. Since most of the elements present in these samples (Fe, Al, Mg, Si and S) showcase a major EELS edge in the 25- 200 eV spectral range, we can perform EELS quantification with a single, fast SI acquisition. This approach offers the potential of a higher signal-to-noise ratio in comparison to the more conventional ionization edges at higher energies, at the expense of a more convoluted spectral analysis.

Methods

FIB lamellas from the Ryugu asteroid were fabricated from Ryugu grains and, subsequently, nanopillars for tomography were created also using FIB. EELS spectrum images were acquired on an FEI TITAN Themis 300 S/TEM, in muti-frame mode (developed in-house), with a dwell time varying between 0.5 and 2 ms and a pixel size ranging from 1 to 2nm. For the tomographic tilt series, EELS spectrum images were acquired at 9 angles ranging from -70 to 70 degrees.

The resulting spectrum images were then analyzed using SVD decomposition of the three- and four-dimensional datasets, blind source separation and curve-fitting EELS quantification.

Results

Figure 1 illustrates the successful EELS elemental mapping of a FIB lamella using curve fitting with enough spatial resolution that allows us to discern the different types of fibers in the phyllosilicate matrix and the characterization of Fe-rich minerals at the nanoscale. This allows to separate the two main phases in the phyllosilicate matrix (saponite and serpentine) by means of EELS analytical tomography.

Conclusion

We present a new method for the EELS analysis of astromineral samples at the nanoscale that, thanks to its dose efficiency, enables unprecedented spatial resolution and EELS analytical tomography on beam-sensitive samples. The method can be extended to other samples presenting EELS ionization edges at low energies. Results show that this technique can provide at least as much information as other microscopy-based techniques like EDX, but with a higher spatial resolution and a fraction of the dose.

Our findings not only provide deeper insights into the structure and chemistry of samples from Ryugu but also show the potential of this methodology for broader application to beam-sensitive astrominerals and geomaterials, such as biominerals.

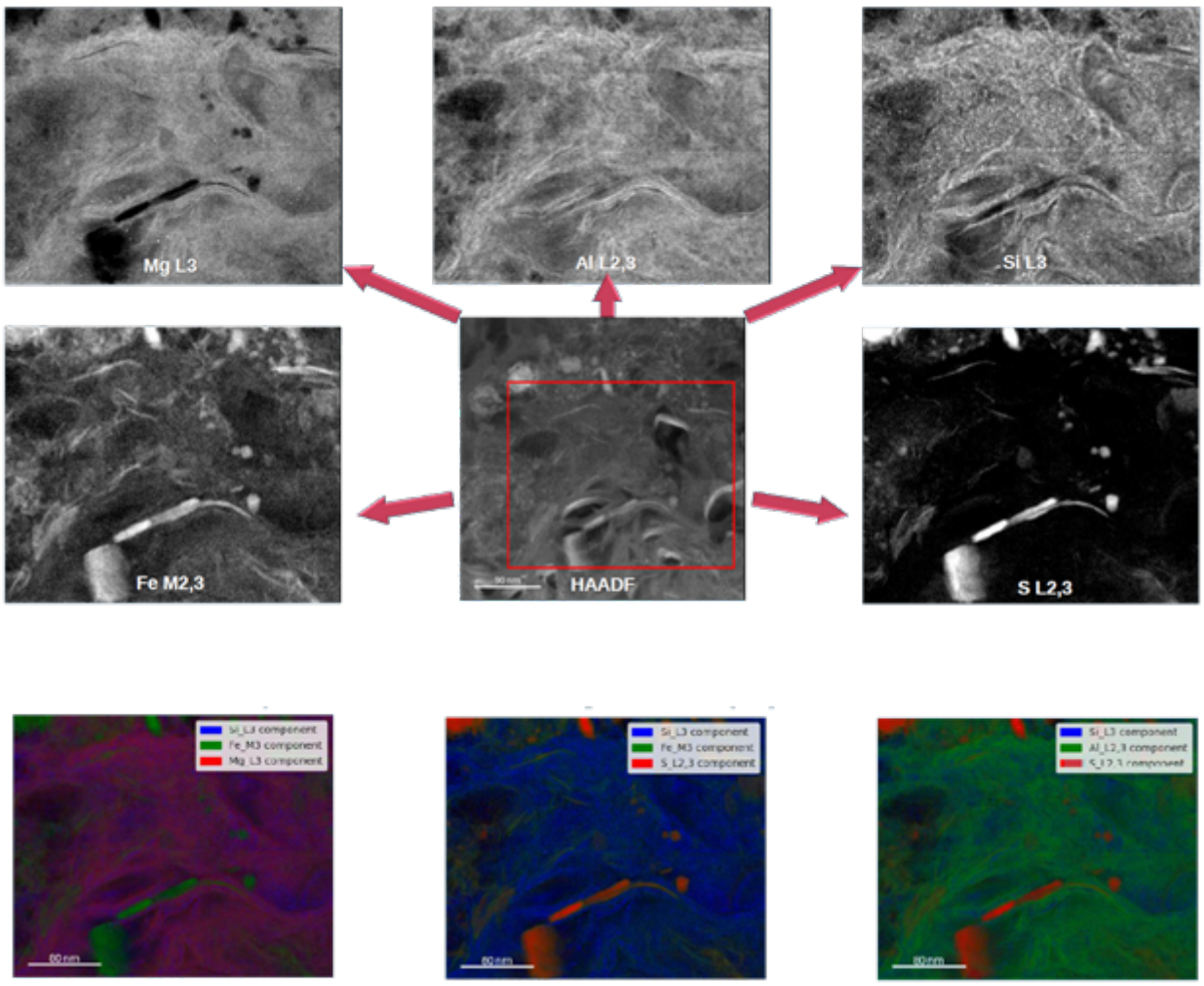

Keywords:

Ryugu, EELS, Tomography,

Reference:

1 K. Kitazato, et al, Science, 2019, 364, 272–275.
2 M. Ito et al, Nat. Astron., 2022, 6, 1163–1171.
3 R. M. Stroud et al, Meteorit. Planet. Sci., 2024, maps.14128.
4 S. Laforet, C. Le Guillou, F. De La Peña, M. Walls, L. H. G. Tizei, M. Marinova, P. Beck, V. T. H. Phan, D. Jacob, B. Mouloud, D. Hallatt, M. Pelaez-Fernandez, J.-C. Viennet, D. Troadec, T. Noguchi, T. Matsumoto, A. Miyake, H. Yurimoto and H. Leroux, Astrophys. J. Lett., 2024, 963, L45.
5 Jacob, D., Marinova, M., Guillou, C. L., Viennet, C., Laforet, S., Leroux, H., Teurtrie, A., Noguchi, T., Matsumoto, T., Miyake, A., Igami, Y., Haruta, M., Saito, H., Hata, S., Seto, Y., Miyahara, M., Tomioka, N., Ishii, H. A., Bradley, J. P., . . . Tsuda, Y. .Meteoritics & Planetary Science.

1051

Multiscale 3D organization of human auditory ossicles unveiled by synchrotron small-angle X-ray scattering tensor tomography

Dr Margaux Schmeltz[1], Dr Christian Appel[1], Ginevra Lautizi[2], Irene Rodriguez Fernandez[1], Torne Tänzer[1], Prof. Dr. Med. Lukas Anschuetz[3,4], Dr Meitian Wang[1], Prof. Dr. Marianne Liebi[1,5,6]
[1]Paul Scherrer Institute, Swiss Light Source, Villigen, Switzerland, [2]Department of Physics, University of Trieste, Trieste, Italy, [3]Otorhinolaryngology Dept., Head and Neck Surgery, Inselspital University Hospital, Bern, Switzerland, [4]Hearing Research Laboratory, ARTORG Center, University of Bern, Bern, Switzerland, [5]Department of Physics, Chalmers University of Technology, Gothenburg, Sweden, [6]Institute of Materials, Ecole Polytechnique Fédérale de Lausanne (EPFL), Lausanne, Switzerland
PS-06, Lecture Theater 1, august 29, 2024, 10:30 - 12:30

Background

The transmission of sound through the human middle ear is a complex process that relies on the biomechanical properties of the ossicular chain, comprising the malleus (hammer), incus (anvil), and stapes (stirrup). These ossicles are the smallest bones in the human body and are responsible for amplifying and efficiently transmitting sound vibrations from the tympanic membrane to the cochlea [1]. Their biomechanical properties are intricately linked to their structure, spanning from the molecular scale (e.g., collagen triple helix) to the millimetric scale (e.g., foramen).
In cases of conductive hearing loss resulting from an impaired ossicular chain, reconstructive surgeries are necessary to restore hearing function. In these procedures, the incus plays a crucial role as either a support for prostheses or as a material to be sculpted itself, serving as an autologous passive implant [2]. However, the optimal positioning of prostheses on the incus and the effects of the carving process on incus biomechanics remain largely unknown and would strongly benefit from an improved knowledge of the ossicles' organization across several length scales.
The ossicles display a hierarchical bone organization, beginning with collagen triple helices that further assemble into fibrils with a periodic d-spacing of approximately 67 nm. These fibrils are mineralized by hydroxyapatite (HA) forming mineral platelets that mostly align with collagen fibrils. However, the shape of these nano-mineral particles and the orientation of collagen fibrils across a significant volume of ossicle, as well as their interactions with the vascular and nutritional foramen network, remain largely unclear to date.
Recently developed Small-Angle X-ray Scattering Tensor Tomography (SAS-TT) has emerged as the preferred method for 3D nanostructural characterization of mineralized tissues like bone over extended spatial regions. SAS-TT combines principles from Small-Angle X-ray Scattering (SAXS), which provides insights into anisotropic non-crystalline structures at sub-um scales, with X-ray tomography, enabling 3D volume measurements. The complete 3D reciprocal space (scattering directions) is reconstructed for each voxel, leading to detailed information about the 3D main orientation and degree of orientation of the set of nano-structures within each voxel.
In this study, our objective is to elucidate the organization of nano- and micro-structures within the human incus, clinically the most crucial auditory ossicles in surgery, using SAS-TT. We aim to gain insights into the preferential orientations induced by sound propagation and identify potential sites of bone remodeling. Additionally, we aim to understand the effect of the sculpting process and erosive pathologies on the inner organization of the incus body.

Methods

Our study includes 5 human incudes in various conditions: 3 healthy, 1 sculpted during ossiculoplasty, and 1 pathological with cholesteatoma, obtained from anonymous donors. The samples were further cut and milled down to a size of approximately 2.5 x 1.5 mm2 each. In the end, the long crus of 2 healthy incudes, and 3 sub-volumes from the body of 1 healthy incus, 1 sculpted incus, and 1

pathological incus, were examined using SAS-TT. The experiments were conducted at the PXI beamline of the SLS (Swiss Light Source, PSI), using a focused beam of 25 x 25 µm² at 12.4 keV and a 4M EIGER detector enabling acquisitions at 300 Hz, resolving a wide energy range. Detector data were reintegrated into 32 azimuthal bins in the range of q = 0.014 – 0.36 Å−1 and symmetrically averaged to eliminate detector gaps. The remaining 16 azimuthal bins were used as input for the SAS-TT reconstructions using the mumott Python library (https://mumott.org).

Results

First results were obtained on the long crus of 2 human incudes. The samples comprised the long process followed by the lenticular process that articulates with the stapes, the last bone of the ossicular chain. We were able to extract the main orientation of the mineralized collagen fibrils and their anisotropy, enabling the identification of 3 regions along the long process that exhibit a higher degree of orientation. These 3 regions with anisotropic collagen arrangement are located along the main vascular channel in the center of the long process, and converge at the bony pedicle, the junction between the long and the lenticular processes.

Further q-resolved analysis revealed the presence of three distinct phases corresponding to various shapes and sizes of mineralized particles within the incus, specifically distinguishing the inner part of the long process from the annular shell around the lenticular process.

Subsequently, we conducted a comparison of 3 incus bodies in various conditions (healthy, pathological and sculpted). The distribution of orientations and anisotropy were extracted for each condition. While no significant differences were observed between the healthy and sculpted samples, the incus body affected by cholesteatoma exhibited a more isotropic collagen fibril organization, with a broader orientation distribution across the sample and lower local degrees of orientation. Additionally, we used the mean intensity as a measure of the mineral density to quantify the prevalence of low-density tissue in the pathological case, suggesting that bone remodeling occurred at different sites.

Conclusions

SAS-TT enables access to structural parameters at both nano- and micro-scales throughout the entire volume of samples. When applied to investigate human auditory ossicles, it revealed anisotropic pathways at the collagen fibril level, which may play a crucial role in guiding sound waves through the bone. Additionally, it identified regions with diverse nano-structuring, pinpointing sites of potential bone remodeling. Furthermore, it shed light on changes occurring in the bone in cases of erosive pathologies such as cholesteatoma. These findings could provide valuable insights for optimizing middle-ear surgery, with wide-ranging benefits for patients with conductive hearing loss.

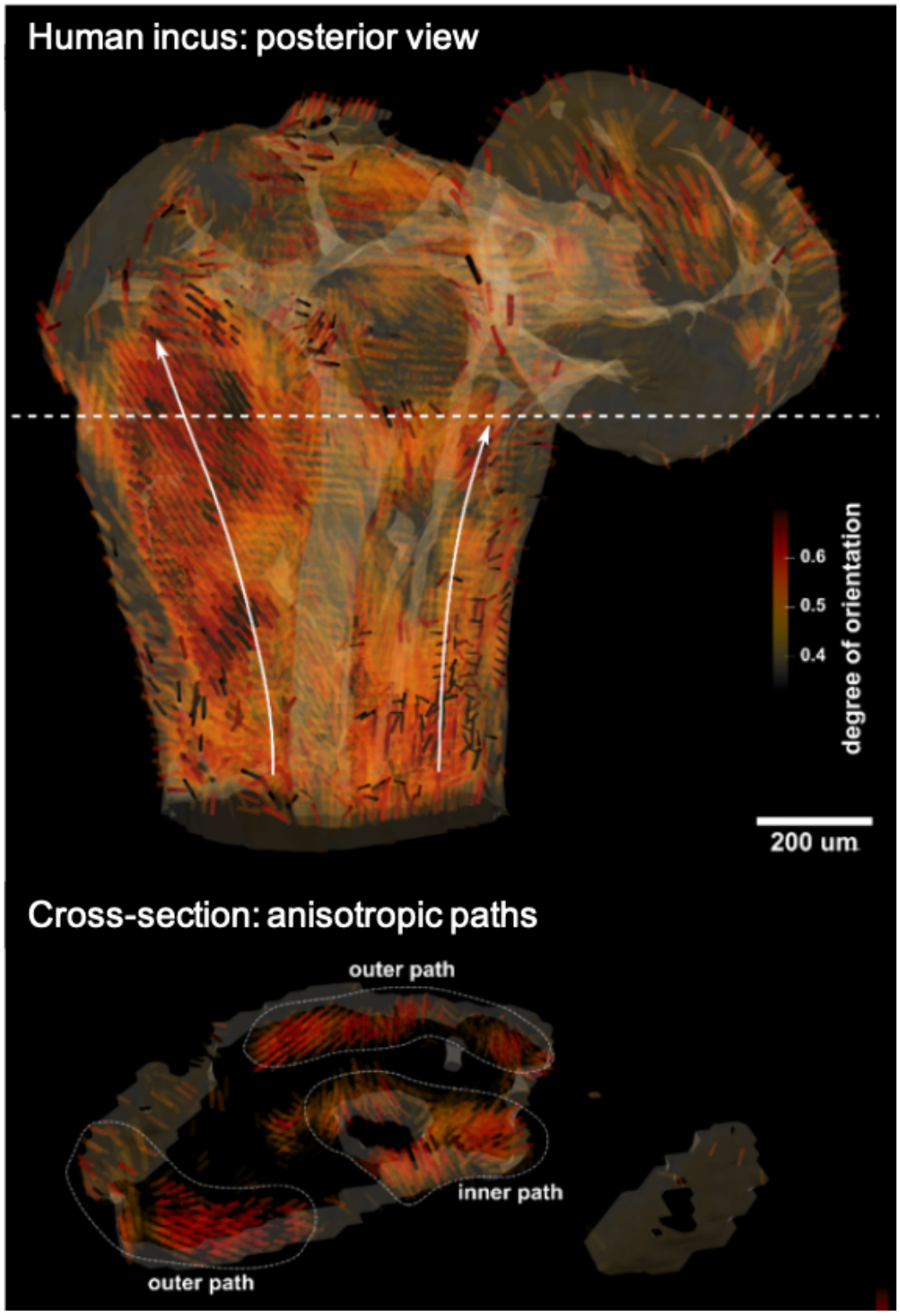

Keywords:

X-ray Scattering, Tomography, Hearing Bones

Reference:

[1] K. B. Hüttenbrink (1992), The mechanics and function of the middle ear. Part 1: The ossicular chain and middle ear muscles, Laryngo-rhino-otologie, 71.11, 545-551.
[2] R. C. O'Reilly et al. (2005), Ossiculoplasty using incus interposition: hearing results and analysis of the middle ear risk index, Otology & Neurotology, 26.5, 853-858.
[3] M. Liebi et al. (2015), Nanostructure surveys of macroscopic specimens by small-angle scattering tensor tomography, Nature, 527, 349-352.
[4] L. C. Nielsen et al. (2023), Small-angle scattering tensor tomography algorithm for robust reconstruction of complex textures, Acta Crystallographica, A79, 515-526.

78

Deep learning 3D-mineral liberation analysis with micro-X-ray fluorescence, micro-computed tomography, and deep learning segmentation

Dr. Patrick Tung[1,2], Amalia Halim[1], Dr. Helen Wang[1], Dr. Anne Rich[1], Dr. Xiao Chen[3], Prof. Klaus Regenauer-Lieb[4], Dr. Christopher Marjo[1]
[1]Mark Wainwright Analytical Centre (MWAC), University of New South Wales, UNSW Sydney, Australia, [2]Research Technology Services, University of New South Wales, UNSW Sydney, Australia, [3]Mineral Resources, Commonwealth Scientific and Industrial Research Organisation (CSIRO), Kensington, Australia, [4]WA School of Mines: Minerals, Energy and Chemical Engineering, Australian Resources Research Centre (ARRC), Curtin University, Kensington, Australia

Poster Group 2

Backgrounds
Mineral liberation has become a key step in the mineral processing industry to quantitatively determine the volume fraction of valuable commodities. Several semi-automated techniques, such as backscattered electron (BSE) images with energy-dispersive spectroscopy (EDS) marketed as commercial systems such as QEMSCAN have been developed for this purpose. However, the extrapolation of the collected 2D data to 3D volumetric remains problematic. Recent developments in X-ray microcomputed tomography (µCT) made it possible to non-destructively characterise these minerals. The problem is the densities of some geomaterials are similar, hence without additional information, it is difficult and often impossible to reliably differentiate the phases just based on µCT data. In this study, we combined the micro-X-ray fluorescence (µXRF) with µCT data and develop a workflow incorporating statistical analysis and deep learning segmentation to interpolate the 2D data into 3D volume (Deep-XFCT).

Methods
The rock used in this study was a fine-grained 24 mm basaltic andesite sample that has a clear and distinct mineral inclusion. A combination of analytical techniques was used for the mineral analysis, which include (1) XRD on powder sample to understand the mineral presence and their abundance, (2) µCT to get 3D volumetric data, (3) µXRF to get elemental mapping for the mineral labels and atomic mass percentages of discrete points for mineral verifications, (4) Raman Spectroscopy to cross check the mineral identifications through µXRF data. The data processing was performed in two steps: (1) establishing ground truth labelling of the mineral phases through µXRF elemental mapping using K-mean clustering, (2) use of the ground truth labelling to train a deep learning model that will segment the mineral phases in 3D µCT data with a specific convolutional neural network architecture specifically designed for image segmentation (U-Net model) using two commercial software Dragonfly ORS and Avizo.

Results
The XRD results provided three prerequisite information for the workflow. First, the mineral phases that exist within the sample that holds important elemental information to correlate with the µXRF data. Second, the number of mineral phases that was presence, which guided the number of clusters for the K-mean clustering. Third, the mineral phases percentage abundance which were used as the validation for the cross-referencing with the K-means clustering abundances and the accuracy of segmentation from the deep learning.
The XRD shows the presence of albite, ankerite, clinochlore, illite, laumontite and quartz. By applying the geochemical principles to the K-means clustering centroids of the µXRF maps, illite, ankerite, and clinochlore can be unambiguously identified through the highest elements concentration present in each mineral. Quartz and albite were identified through the µXRF point analysis by the highest Si and

Na mass percentage, respectively. Laumontite did not have a unique elemental identifier nor characteristic combination of elements and was identified by deduction as the final element. Raman Spectroscopy was able to confirm the presence of albite, clinochlore and quartz.
The minerals assigned to each pixel of the µCT orthoslice on the top and bottom surface of the sample where a U-Net neural network model was trained to segment the µCT based on the mineral labels. From visual analysis, the model captured the major contours of the mineral phases. This includes separating the albite and illite matrix to a good approximation, despite their identical grayscale value. However, the model failed to recognise the finer details apparent in the labelled training data. The overall accuracy from all minerals for top and bottom surfaces from the U-Net model in Dragonfly ORS 2021.2 were 70.23% and 69.56%, respectively. Furthermore, the results from the U-Net model in Avizo 2021.1 were similar with 73.57% and 72.08% for the top and the bottom surfaces. To validate the segmentation from the model, the sample was cut 5mm from the top and bottom of the plug and the surfaces were subsequently mapped with µXRF to allow the mineral phases maps within the volume of the sample to be compared. In comparison to the training data, the validation data has lower but serviceable accuracy. Using the phase identification as labels, a neural network was successfully trained to segment other slices throughout the volume to obtain a 3D representation of the mineral phases in the sample.

Conclusions
Our results successfully demonstrate semi-automated multi-modal analysis with an approach that is universal to any multi-instrument approach. The blend of µXRF and µCT provides a unique opportunity for robust 3D mineral liberation analysis in both field and laboratory applications when combined with Deep-XFCT. While Deep-XFCT did not provide pixel-level accurate segmentation, it was able to provide an excellent proxy for the purposes of obtaining the presence, location, distribution, and morphology of grains dispersed throughout a core plug. It was also shown that Deep-XFCT was able to differentiate fine-grained minerals of similar density that would be impossible by manual segmentation. This technique is a valuable technique that has the potential to expedite 3D mineral liberation analysis.

Keywords:

Deep learning, Image analysis, Multi-modal

193

Nanoscale arrangement of the healthy dentin and comparison with the dentino-genesis imperfecta-affected dentin

Dr Maxime Vallet[1,2], Dr Margot Riou[3], Mme Margot Leclercq[1], Dr Elsa Vennat[1]
[1]Université Paris-Saclay, CentraleSupélec, ENS Paris-Saclay, CNRS, LMPS, Gif-sur-Yvette, France , [2]Université Paris-Saclay, CentraleSupélec, CNRS, SPMS, Gif-sur-Yvette, France, [3]Universite de Paris, Dental Faculty, Paris, France

Poster Group 2

1. Introduction/Background

The tooth, mainly composed of dentin, which lies between enamel and pulp, is the hardest organ in the human body. Dentin is a mineralized collagen framework comprising 70% carbonated hydroxyapatite, 20% organic matrix (mainly type I collagen forming collagen fibrils), and 10% water. The tooth's necessary mechanical resistance without causing it to fracture comes from its particularly complex micro- and nano-structural organizations. Dentinogenesis Imperfecta (DI) is a rare genetic disease that causes severe dentin hypomineralization and damage to its structure (de la Dure-Molla, 2015). In some cases, DI is caused by a type I collagen mutation (Yamaguti PM, 2023), which leads to the modification of dentinal tissue organization at the nanoscale and microscale. Clinically, it can lead to rapid attrition of the dentin tissue, eventually leading to tooth loss, probably due to lower mechanical properties. In this study, we present an original analysis of the nanostructure of the healthy dentin compared to dentin affected by DI. A focus on collagen fibrils and hydroxyapatite entanglement in both samples has been performed from transmission electron microscopy (TEM) techniques.

2. Methods

Both permanent and deciduous teeth with no visible pathological signs were prepared for the control samples. In contrast, a deciduous molar was chosen for pathological dentin from a patient diagnosed with DI exhibiting damage to type I collagen. All samples were sectioned from the crown to the root and mechanically polished using abrasive Si-C paper with decreasing grain size. The samples were then dehydrated progressively through a series of increasing ethanol concentrations. TEM samples were then prepared in the different samples at different location in teeth by using a FEI ThermoFisher Helios Nanolab 660 focused ion beam. The obtained sections were observed with a FEI ThermoFisher TITAN3 G2 80-300 transmission electron microscope equipped with a Cs probe corrector given a 0.07nm spatial resolution and a SuperX detector for energy dispersive X-rays spectroscopy (EDX) analyses.

3. Results

Using HR-(S)TEM techniques, the microstructure of the healthy dentin has been studied at different scale close the enamel and in the middle dentin. Collagen fibrils and hydroxyapatite crystals are completely tangled. While fibrils looks like long cylinders with sizes over than hundreds of nanometers, crystals are usually smaller than 5 nm in length and it seems that they are roughly aligned with the direction of collagen fibrils.
Let’s first focus on collagen fibrils. The analysis of their diameter revealed that collagen fibrils tends to shrink as they are close to the enamel. Their distribution in the intertubular dentin also appears to be different close the enamel and in the middle dentin. The collagen fibrils are organized in a more isotropic way near enamel than in middle dentin where they are lying in planes perpendicular to the tubule axis. In those planes perpendicular to tubule axis, bundles of collagen fibrils and mineral are oriented in preferential directions, creating a woven structure.

Concerning the hydroxyapatite crystals, we observed that they are organized in S-shaped structure composed of individual HAP crystals and parallel to the adjacent fibrils. The individual crystals are mainly elongated along their c-axis but can also be elongated along a- and b- axis. This organization looks similar regardless of the location in the dentin.
In comparison, DI dentin look very different. The density of collagen fibrils drastically drops compared to the one in the healthy dentin. At the opposite, hydroxyapatite crystals are much denses and their distribution looks homogeneous. Looking at individual crystals' size, we did not observe any statistical difference between healthy dentin and dentin affected by DI. With the EDS analysis, we found Ca/P ratios approximatively at 1.67 (ideal hypothetical value in hydroxyapatite crystals), with a tendency to lower values in dentin affected by dentinogenesis.

4. Conclusions
At the nanoscale, dentin shows a complex and anisotropic organization involving a mineral phase made of hydroxyapatite crystals and an organic phase mainly made of collagen fibrils. In this work, we firstly analyzed precisely the microstructure of dentin according to the location in the tooth and with cross-sections parallel or perpendicular to the tubular paths thanks to the combination of FIB and TEM. The comparison of the healthy dentin and the DI one brings new insight into the tooth formation.

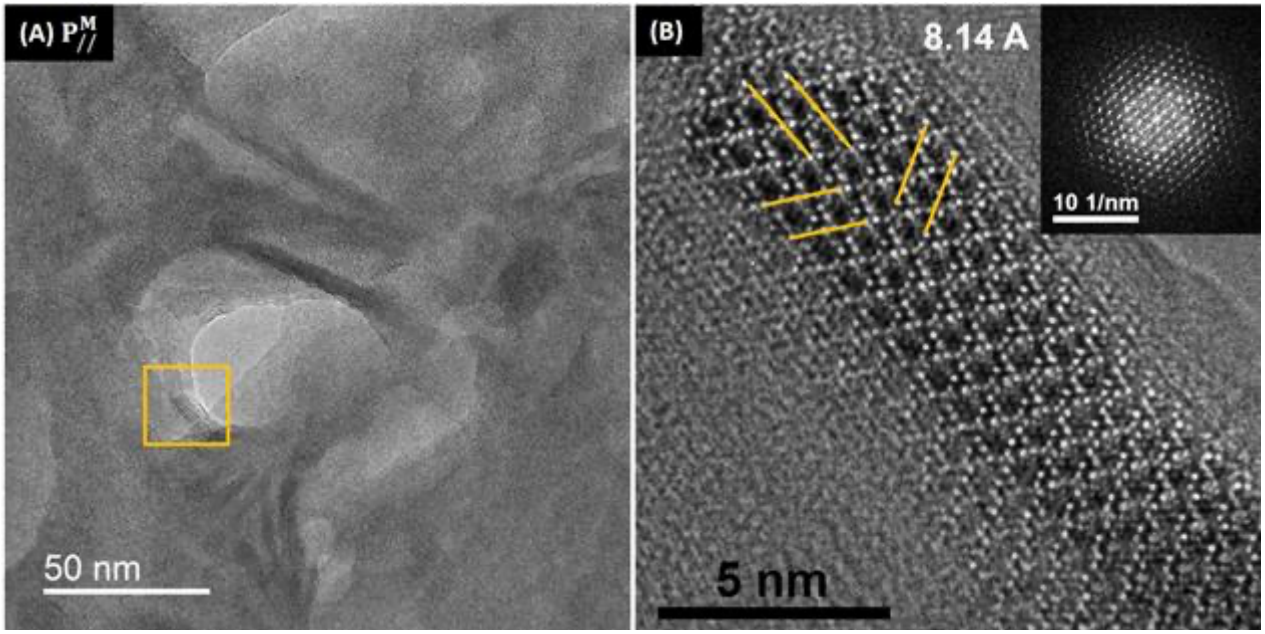

Keywords:

bio-minerals, architectural materials, (S)TEM

Reference:

De La Dure-Molla M et al. Isolated dentinogenesis imperfecta and dentin dysplasia: revision of the classification. Eur J Hum Genet. 2015
Yamaguti PM et al. Unequal Impact of COL1A1 and COL1A2 Variants on Dentinogenesis Imperfecta. J Dent Res. 2023

212

Electron microscopy characterization of king scallop (Pecten maximus) shells from low-voltage SEM to 3D-EBSD reconstruction

Dr Lise Guichaoua[1], Dr Benazir Khurshid[3], M Arnaud Benchetrite[3], Ms Stéphanie Bessette[1], Dr Bryce Stewart[2], Pr Natalie Reznikov[3], Pr Roland Kröger[4], Pr Raynald Gauvin[1]
[1]McGill Electron Microscopy Research Group, Department of Mining and Materials Engineering, McGill University , Montreal, Canada, [2]Marine Biological Association, Plymouth, United Kingdom, [3]Department of Bioengineering, Faculty of Engineering, McGill University, Montreal, Canada, [4]School of Physics, Engineering and Technology, University of York, York, United Kingdom

Poster Group 2

Background

The shell of the bivalve Pecten maximus, also called the king scallop, was previously found to be detrimentally affected by the presence of metal contamination, in particular Cu, Pb, and Zn originating from mining activities on the Isle of Man [1]. In addition to a reduction of shell thickness, scallop shells from the contaminated area exhibit a sharp break line in the mineralization within the foliated region of both the top and bottom valves. Our data suggest that these mineralization break line caused reduced fracture strength compared to pollution-free scallops, which results in increased mortality due to predation and during the process of dredging. These break lines have already been referred to as being of aragonitic prismatic structure [2].
To shed light on the possible impact of metal contaminations on the growth and strength of scallop shells and in particular on the 3D morphology and microstructure of the scallop, from contaminated and uncontaminated sites, we used characterization tools at different length scales (from cm to µm) using electron and X-ray probes to determine areas of interest in contaminated and healthy (uncontaminated) shells to finally realize crystallographic orientation map using EBSD technique and localized 3D reconstruction by focused ion beam techniques (FIB). The aim of this study was to combine these techniques to produce a full 3D EBSD map of the crystallographic orientations of the critical zones.

Methods

The scallop samples were cut using a diamond cut-off wheel (South Bay Technology Low Speed Diamond Wheel Saw MODEL 650) to extract a large cross-section of contaminated and healthy scallop to study the whole shell section. The cross-sectioned samples were then polished with lapping pads to a felt disk with a 50 nm colloidal silica suspension, to obtain a perfectly flat surface for future SEM observations and EBSD analysis.
We first applied 3D X-ray microscopy using micro-computed tomography (microCT) scanning with a ZEISS Xradia 520 Versa X-Ray microscope, at different resolutions to locate potential structural defects or the mineralization break line on contaminated shell and healthy shell.
The same samples were then analyzed by scanning electron microscopy (SEM) coupled with elemental analysis by energy dispersive X-ray spectroscopy (EDS) to detect differences of microstructure or orientation on the shell cross section. The equipment used for this purpose is a Hitachi field emission gun (FEG)-SEM SU8230 with low voltage analysis (3KeV) by secondary and backscattered electrons (PD-BSE) imaging, Bruker XFlash EDS detector for elemental quantification point analysis, and Bruker Flat Quad detector for EDS mapping analysis. A 10 nm layer of carbon coating was necessary to be able to run long EDS mapping acquisition.
Electron Backscattered Diffraction analyses were conducted for both types of samples on a SU3500 SEM from Hitachi under VP-SEM mode at 20keV on main areas detected by the previous SEM analyses.

The FIB tomography is performed using a Hitachi Ethos NX5000 FIB-SEM to obtain a stack of images and the Dragonfly software from Comet [3] to build the 3D volume samples from each type. In addition, the FIB-SEM NX5000 is equipped with a Symmetry S2 EBSD camera from Oxford Instruments that can allow us to obtain stacks of EBSD maps to build 3D volumes with crystallographic orientation information.

Results

MicroCT analyses carried out at different resolutions (from 30 µm to 2.5 nm pixel size) have shown that the break line visible in the contaminated shell is also present in healthy shells, but less marked and finer than that observed in the contaminated shell. These lines extend across the entire shell surface, although their point of initiation remains a mystery.

SEM analysis enabled us to observe the variation in microstructure across the entire cross-sectional area and to determine the zones of interest for the different microstructures observed in each type of shell. The zone we call the "break line" presents a prismatic microstructure as expected, different from the microstructure observed in the main parts of the shell, largely composed of elongated and foliated grains. In addition, a detailed analysis of the samples revealed the presence of a main prismatic layer, which was found to be thicker in the contaminated samples, and we were also able to observe several thinner prismatic layer in both types of sample.

EBSD analyses, carried out on various zones of interest selected from SEM observation, confirmed that the foliated microstructure is calcite. We detected that the prismatic layer was indeed clearly well-crystallized aragonite for the disruptive line. EBSD maps obtained in regions containing thinner disruptive layers reveal that there is no detection of specific crystallographic orientation.

Conclusion

The combination of microscopy techniques using electron probes and X-rays at different length scales has enabled us to gain a better understanding of the structure of scallop shells and the impact of metal contamination from mining on the Isle of Man.

After a detailed study using microCT and low voltage SEM, targeted EBSD analyses revealed that the break lines present over the entire shell surface in all shells are prismatic in structure and are associated with the aragonitic myostracial layer, while the rest of the shell is predominantly composed of calcite with a foliated microstructure. This aragonitic layer, well crystallized in its thickest zone according to EBSD results, shows no detectable crystallization in its thinnest zone. A more in-depth study of these areas would help determine the cause of this lack of identification.

EBSD mapping acquired with the FIB-SEM NX5000 will enable us to obtain 3D volumes with crystallographic orientation information for healthy and contaminated shells, allowing us to compare growth and development of each type of scallop and detect defects in shell crystallization depending on their environment.

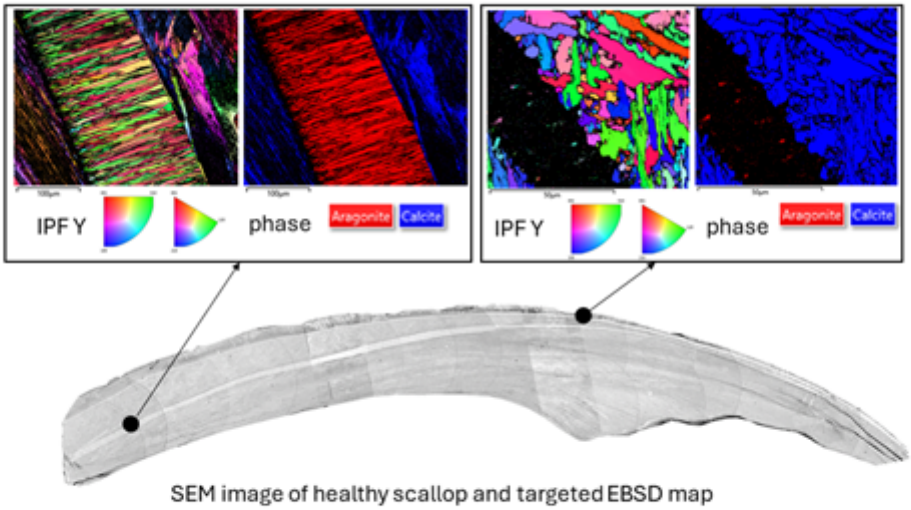

SEM image of healthy scallop and targeted EBSD map

Keywords:

Scallops, SEM-FEG, EBSD, 3D-FIB, 3D-EBSD

Reference:

1. Stewart, B.D., et al., Metal pollution as a potential threat to shell strength and survival in marine bivalves. Science of The Total Environment, 2021. 755: p.143019.
2. Grefsrud, E., et al., Modifications in Microstructure of Cultured and Wild Scallop Shells (Pecten maximus). Journal of Shellfish Research, 2008. 27: p.633-641.
3. Dragonfly. 2022, Comet Technologies Canada Inc.: Montreal, Canada,.

267

From Tarquinia's Necropolis to biorestoration: the role of the characterization in a multidisciplinary research context

Francesco Mura[1,2], Francesca Benedetti[3], Matilde Kratter[3], Luca Buccini[1], Pierfrancesco Atanasio[1], Anacleto Proietti[1], Angela Cirigliano[3], Daniele Passeri[1,2], Teresa Rinaldi[2,3], Marco Rossi[1,2]
[1]Department of Basic and Applied Sciences for Engineering (SBAI), Sapienza University of Rome, Rome, Italy, [2]CNIS-Center for Nanotechnology Applied to Industry of Sapienza, Sapienza University of Rome, Rome, Italy, [3]Department of Biology and Biotechnologies “Charles Darwin”, Sapienza University of Rome, Rome, Italy

Poster Group 2

Background incl. aims
Moonmilk is a secondary calcite deposit often found in karst caves, formed by nanofibers of biogenic origin, mostly on calcarenite surfaces, in high humidity and low temperature conditions. Recently, in the ancient Etruscan hypogean tombs of the necropolis of Tarquinia, moonmilk has been identified in a white patina covering the wall paintings. The presence of bacteria, promoting the calcium carbonate deposition, has opened the way to their potential use as a new and promising way for biorestoration. Our aim is to optimize this process for a successful and stable calcite deposition, because the conservation of the hypogean environment is a real challenge for restorers and conservators, and it requires a strong characterization work, both from a biological side, for the selection of the best bacteria producers of calcite, and from the applied methods, microscopies or spectroscopies, to establish a safe protocol for the evaluation of the deposited calcium carbonate and its application as an innovative restoration material in cultural heritage.

Methods
Optical microscopy, scanning electron microscopy (SEM), transmission electron microscopy (TEM) and atomic force microscopy (AFM) were used to characterize the calcite morphology, while its crystallinity was assessed using X-Ray Diffraction (XRD), Raman spectroscopy. Metagenomic studies were carried out to identify the complete bacterial community present in the moonmilk, while the choice of the most promising species capable of rapidly depositing calcium carbonate under specific conditions was performed by selecting single strains through culture-dependent method.

Results
Our research has covered all aspects of moonmilk biogenesis, from structural to microbiological studies. In our previous work we have described how Moonmilk formation occurs not only on the outer surface of the rock, but also in the inside, and how the interaction between bacteria and the rock substrate can influence the final morphology of the calcium carbonate precipitates, showing structures at both the nano- and micro-scales. Moonmilk can also be seen as a biosignature in the field of astrobiology, while for biotechnological applications, the study of the microbial community has allowed the selection of different species capable of rapidly producing calcium carbonate, making them suitable for bioconsolidation intervention.

Conclusion
Although the chemical reactions that elongate moonmilk nanofibers have yet to be determined, their origin is certainly biogenic, characterized by the presence of an entombment structure produced by a bacterial strain that detoxifies calcium ions by producing calcium carbonate. Environmental conditions and rock substrates also have a strong influence on the final shape of moonmilk crystals. Nevertheless, the analysis of the microbial communities in the Etruscan hypogean tombs has

demonstrated their very fundamental role, which can be used as a green and innovative source for bioconsolidation interventions.

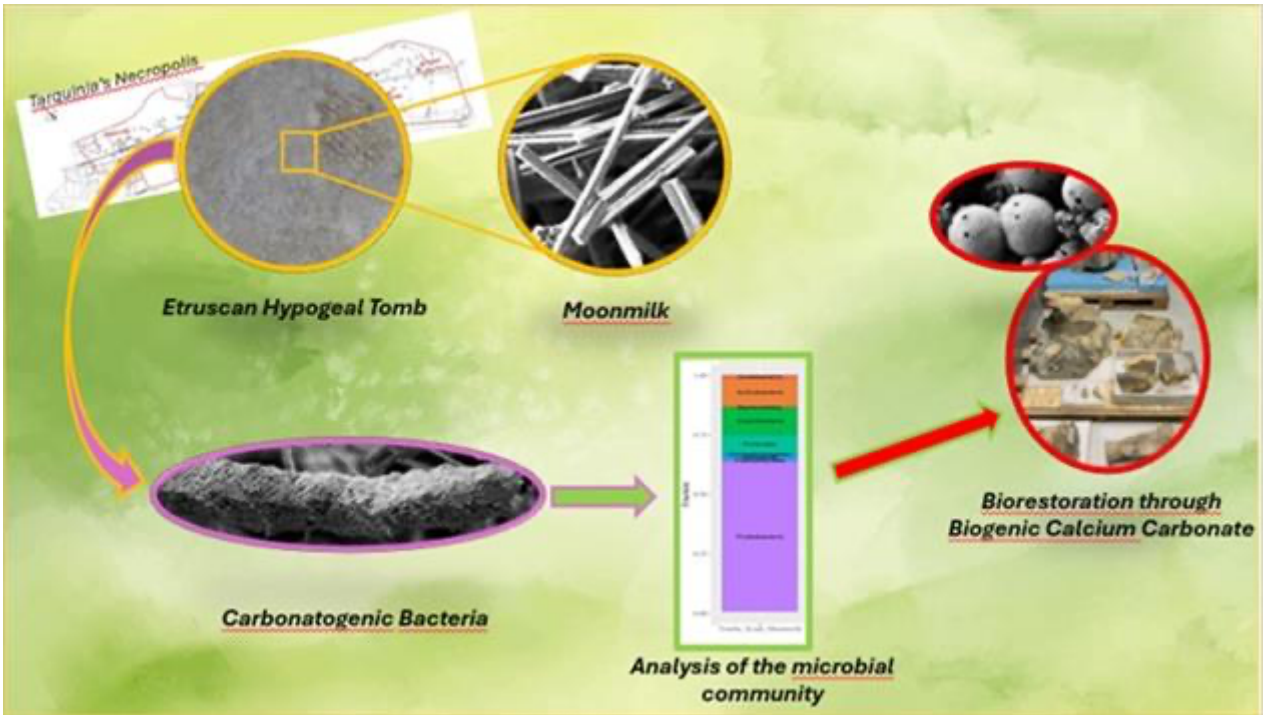

Keywords:

Moonmilk, calcium carbonate, biorestoration

Reference:

Tomassetti, M.C. et al. SciRep 7, 6027 (2017).

Cirigliano, A. et al. SciRep 8, 15839 (2018).

Cirigliano, A. et al., Environ Microbiol 23, 3957-3969 (2021).

Ronca, S., et al. Biogeosciences, 20, 4135–4145 (2023).

Benedetti, F., et al. Journal of Cultural Heritage 64, 282-289, (2023).

388

Correlating absorption and diffraction contrast tomography on earth and space materials

Olivia Barbee[1], Jette Oddershede[1], Matthew Pankhurst[2], Florian Bachmann[1], Stephen Hall[3], Jonas Engqvist[3], Rhian Jones[4], Anders Svensson[5], Erik Lauridsen[1], Jun Sun[1]
[1]Xnovo Technology ApS, Køge, Denmark, [2]ITER/INVOLCAN, Tenerife, Spain, [3]Lund University, Lund, Sweden, [4]The University of Manchester, Manchester, UK, [5]University of Copenhagen, Copenhagen, Denmark

Poster Group 2

Background incl. aims
Minerals in polycrystalline rocks on Earth have formed over durations spanning solar system formation up to our present geosphere and cryosphere. The conditions of rock and ice formation are recorded in the relative crystallographic orientations, sizes, shapes, defects, and distributions of their crystals or grains that, together with chemistry, chronicle planetary dynamics over timescales of seconds to billions of years. The three-dimensional (3D) mineral architectures are therefore fundamental to understanding celestial bodies and the solid earth, while providing crucial context within which we explore the origins of life on our planet and the interactions between its cryosphere, biosphere, and atmosphere. Observations, however, have long been restricted by 2D analyses and the destructive sample preparation required for 2D analytical techniques, as well as an inability to directly observe textural or mineralogical evolution. Maintaining 3D and time-dependent contexts of microstructures is vital to fully understand the dynamic formation and efficient exploitation of earth materials, both as recorders of earth processes and to support environmentally sustainable innovation.

Methods
Minerals are defined by both composition and crystallographic structure. X-ray absorption contrast tomography (ACT) is ideally suited to derive information on porosity and to characterize boundaries between higher- and lower-density phases. However, many minerals have similar X-ray attenuation, and some mineral systems have little or no variation in mineral type (e.g., ice), leading to minimal image contrast. Complimentary to ACT, lab-based diffraction contrast tomography (DCT) produces 3D maps of the grain morphologies and crystallographic orientations for the different constituent phases. ACT and DCT, both non-destructive in nature, can be performed on the same micro-CT system, and combining the two can provide earth and planetary scientists with unprecedented new knowledge – in 3D – while keeping the often rare or precious samples intact.

Results
We present different examples of combined ACT and DCT studies on earth and space materials to illustrate some of the current imaging capabilities. Results from an olivine chondrule inside a carbonaceous chondrite, a type of meteorite that can host organic compounds thought to contain the ingredients for life, reveal previously unobserved relationships between grain shape, size, composition, and chemical zoning that inform models of melting during short heating events in the proto-planetary disc. Ice is also explored with the goal of characterizing the 3D microstructural and porosity evolution of glacial ice, which contextualizes chemical and isotopic measurements used to extract climate records from ice cores.

Conclusion

Together, quantitative ACT and DCT can be combined to create 3D petrography: a non-destructive method of identifying and characterizing multiphase materials (rocks, alloys, etc.) without a priori knowledge. As a step towards that goal, this work is developing the utilization of joint ACT and DCT in addressing different challenges in geoscience.

Keywords:

Lab-based DCT, absorption contrast tomography

563

Carbonaceous inclusions from the oldest sediments on Earth

Magnus Harding[1,2], Austin Jarl Boyd[1], Sandra Siljeström[3], Madina Shamsuyeva[4], Pooyan Aliuos[4], Minik Rosing[1], Tue Hassenkam[1]
[1]Globe Institute, University of Copenhagen, Copenhagen, Denmark, [2]Sino-Danish College (SDC), University of Chinese Academy of Sciences, Beijing, China, [3]RISE Research Institutes of Sweden, Stockholm, Sweden, [4]Institute of Plastics and Circular Economy IKK, Leibniz University Hannover, Hannover, Germany

Poster Group 2

Background incl. aims:
The Isua Supracrustal Belt in Southwest Greenland contains rocks which are at least 3.7 billion years old, and are among the oldest rocks on Earth. Sediments found here display contiguous horizons of carbonaceous material parallel with sedimentary bedding planes (Rosing 1999). This material, present as graphitic carbon, has been proposed to be some of the oldest remnants of life on Earth, inferred based on its mode of occurrence, carbon isotope ratios, its association with heteroatoms such as nitrogen, oxygen, phosphorous and iron, and from the nanoscale crystal structure (Ohtomo et al. 2014, Hassenkam et al. 2017), evidence which is all compatible and together suggestive of an origin of the graphitic material as biogenic pelagic detritus.
In certain places, the graphite is enclosed in secondary metamorphic minerals such as garnets. This graphite occurring as inclusions has been targeted by previous studies, which also identified certain viscous fluid inclusions. The study presented attempts to characterize the chemistry of these fluid inclusions occurring alongside the graphitic material within garnet porphyroblasts.

Methods:
In this study, the liquid inclusions are accessed by breaking open the garnets and their residues are subsequently characterized using atomic force microscopy (AFM), as well as infrared spectroscopy coupled to AFM (NanoIR). Optical photothermal infrared spectroscopy (O-PTIR) and time-of-flight secondary ion mass spectrometry (ToF-SIMS) are also used to characterize the chemistry of the inclusion residues and to assess their association with the solid graphitic inclusions.

Results:
Using AFM-based infrared spectroscopy, we obtain infrared absorption spectra from just the inclusion at a high spatial resolution. The liquid inclusion residues are ubiquitously characterized by infrared absorption at wavenumbers 1280 cm-1 and 1660 cm-1, interpreted as the C-N and C=O vibrational absorption from amide-like functional groups. Similarly, ToF-SIMS shows secondary species containing C, N and O from the inclusion residues. O-PTIR shows how the amide-like infrared absorption signal can be traced along horizons of graphitic material.

Conclusion:
This study shows how infrared spectroscopical methods coupled to optical and scanning probe microscopy methods can be used to characterize the chemistry of minute domains of ancient carbonaceous material occurring as inclusions in garnet porphyroblasts. The observations from NanoIR were corroborated by ToF-SIMS analyses. Together, these methods indicate that the carbonaceous material consists of C, N, and O-rich material in an amide-like configuration.
The chemistry of the inclusions is consistent with that which would be expected from degraded biogenic matter. Together with previous studies, this is highly suggestive of a biological origin for the carbonaceous material found in the oldest sediments on Earth.

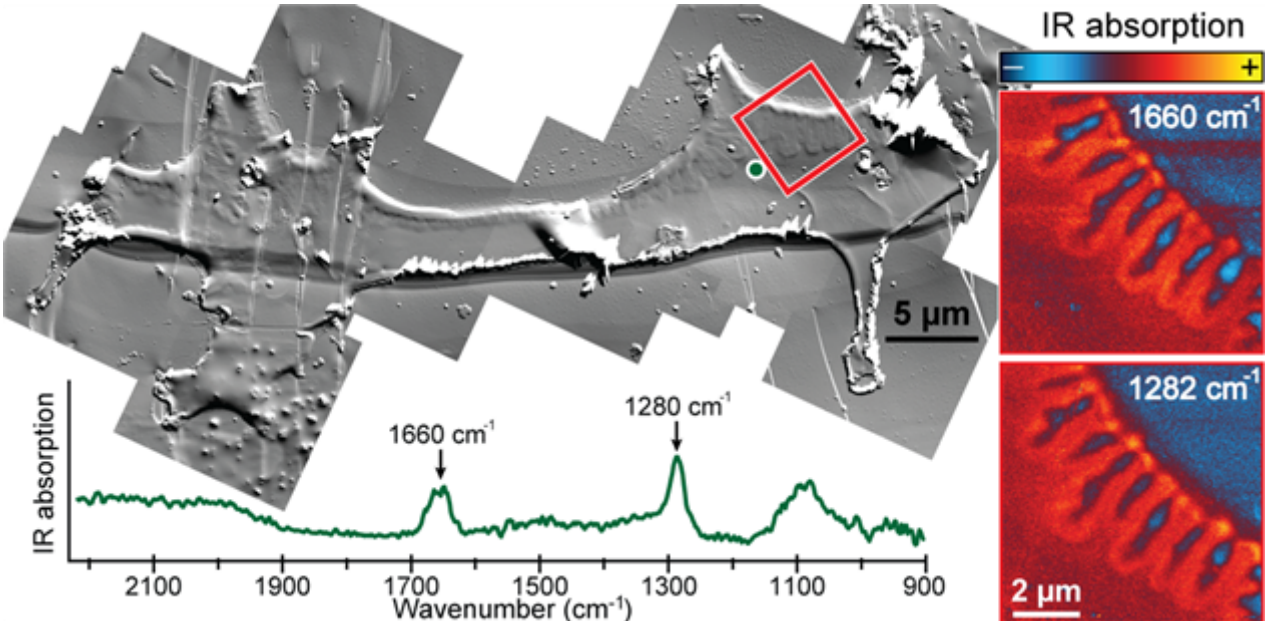

Keywords:

AFM, IR-spectroscopy, ToF-SIMS, early life

Reference:

Rosing, M.T., 1999. 13C-depleted carbon microparticles in ≥3700-Ma sea-floor sedimentary rocks from west Greenland. Science 283, 674–676. https://doi.org/10.1126/science.283.5402.674
Ohtomo, Y., Kakegawa, T., Ishida, A., Nagase, T., Rosing, M.T., 2014. Evidence for biogenic graphite in early Archaean Isua metasedimentary rocks. Nature Geoscience 7, 25–28. https://doi.org/10.1038/ngeo2025
Hassenkam, T., Andersen, M.P., Dalby, K.N., Mackenzie, D.M.A., Rosing, M.T., 2017. Elements of Eoarchean life trapped in mineral inclusions. Nature 548, 78–81. https://doi.org/10.1038/nature23261

841

The EXCITE² Network: a European infrastructure providing transnational access to leading-edge imaging facilities

Alireza Chogani[1], Oliver Plümper[1], Geertje ter Maat[1], the EXCITE team
[1]Department of Earth Sciences, Utrecht University, Utrecht, The Netherlands

Poster Group 2

The EXCITE² Network is a leading European electron and X-ray imaging infrastructure for research into Earth materials. This network is revolutionizing Earth and environmental material science research by consolidating 19 research facilities in 12 European and associated partner countries into a unified infrastructure that will provide transnational access to advanced imaging technologies. This open access to our state-of-the-art microscopy facilities enables scientists to decipher complex processes within Earth materials across scales ranging from nanometres to hundreds of centimetres. Understanding these processes is critical to creating a sustainable, carbon-neutral society, as they govern various phenomena, including environmental toxicity and its impact on human health, critical metal extraction for renewable energies, geothermal energy extraction, subsurface energy storage, and the utilization of Earth materials for long-term storage of climate-altering gases.
EXCITE² is driving interdisciplinary collaboration and cross-fertilisation across academic institutions, scientific disciplines, and industry, propelling Europe towards a sustainable future. In addition to access to leading-edge imaging facilities, the network offers early career researchers a chance to team up with leading Earth-materials scientists, develop new collaborations, engage in cross-disciplinary initiatives, and execute progressive electron and X-ray imaging projects that contribute to the advancement of Earth-materials research. We connect with you, provide access to workshops and webinars, assist in preparing your proposals for facility access, and actively support your research goals. Moreover, the initiative offers dedicated training programmes to a new generation of researchers within the European open science landscape. EXCITE² is introducing innovative service developments, such as artificial intelligence and leading-edge imaging experiments, to increase the user's problem-solving capacity. As such, EXCITE² is paving the way towards a sustainable future, driving scientific excellence, and creating positive societal impact.
Access to EXCITE² can be requested by applying to our transnational access calls. Interested? Have a look on our website (https://excite-network.eu) – and apply for the next call!

Keywords:

EXCITE, Transnational access, Electron microscopy

844

Thallium and arsenic incorporation in roméite group minerals

Priv.-Doz. Dr. Tamara Đorđević[1,2], Priv.-Doz. Dr. Michael Stöger-Pollach[1], Dr. Sabine Schwarz[1]
[1]E057-02 USTEM, Vienna University of Technology, Vienna, Austria, [2]Department of Mineralogy and Crystallography, University of Vienna, Vienna, Austria

Poster Group 2

Background incl. aims
Roméite group minerals (RGM) are oxides, which belong to the large pyrochlore supergroup of minerals. The general formula of the pyrochlore supergroup is $A_2B_2X_6Y$ (A = Na, Ca, Ag, Mn, Sr, Ba, Fe(II), Pb, Sn(II), Sb(III), Bi(III), Y, REE, Sc, U, Th, □ and H_2O, B = Ta, Nb, Ti, Sb(V), W, V(V), Sn(IV), Zr, Hf, Fe(III), Mg, Al, and Si, X = O, OH, or F and Y = (OH)–, F–, O2–, □, H_2O, or even large cations, such as K, Rb, Cs). The crystal structure of RGM is build-up of BO_6 octahedral framework that forms tunnels along [110] where 8-coordinated A cations and Y anions are hosted. In the RGM, Sb(V) is the dominant cation at the B site, but on the A-site, larger cations can be incorporated where also the ion-exchange can take place. Therefore, RGM are often used for the immobilization of the toxic metals, such as Pb and Sr and have been frequently reported as weathering products in mining wastes and smelting residues resulting from Sb mining activities.

Methods
High-resolution electron microscopy, both transmission (TEM) and scanning (SEM), including energy dispersive spectroscopy (EDS), energy electron loss spectroscopy (EELS), and selected area electron diffraction (SAED), are used to characterize Sb- and As-rich samples from mining waste dumps from the Sb-As-Cr Lojane deposit, North Macedonia, and Tl- and Sb-rich samples from weathered technosols of the central part of the Sb–As–Tl–Au Allchar deposit, North Macedonia. These techniques are supplemented by X-ray diffraction (XRD) and Raman spectroscopy.

Results
RGM from the Lojane deposit are observed as extremely thin (< 10 µm) weathering crusts encircling grains of stibnite, Sb_2S_3 and realgar, AsS. Larger homogenous grains up to 500 µm are formed by Sb-dominant variants of this oxide, which are also characterized by broad dehydration cracks, indicating that they were originally formed as gels. The analysed thin crusts and aggregates are most likely poorly crystalline to amorphous, As-dominant RGM-like phases, which appear darker grey in the SEM images, and nano- to microcrystalline, Sb-dominant RGM, which appear very light grey in the SEM images. The crystallographic position of arsenic in the RGM in our samples is not fully clear. In the RGM, As(V) may occupy the octahedrally coordinated A-position, but it strongly prefers tetrahedral coordination. The distorted cubic B-position in RGM is too large for the As(V) cation. These crystal-chemical preferences explain why the As is mostly in the X-ray amorphous phases. However, EDS point analyses clearly document that the RGM may incorporate considerable As.
In the mining waste dumps of Allchar deposit, Tl dissolved during weathering is besides other Tl-oxides, such as avicennite, Tl_2O_3 and amorphous Tl-Mn-oxides, reprecipitated as tiny spherulitic aggregates (up to 2 µm) of a Tl-Sb-oxide (a new mineral species). TEM-based SAED on Tl-Sb-oxide nano-particles confirmed that the Tl-Sb-oxide is crystalline, and chemical composition analysed by EDS-line and area scans confirmed a Tl:Sb ratio of 2.5. The cell parameters calculated from the SEAD pattern show good comparison with the members of pyrochlore-type structure.

Conclusion
Understanding the potential pathways for Tl and As incorporation in pyrochlore-type structures addresses not only the growing environmental concern over these two priority pollutants, but also contributes to the larger field of waste management.

Financial support of the Austrian Science Fund (FWF) [P 36828-N] is gratefully acknowledged.

Keywords:

thallium, arsenic, mining wastes, nano-minerals

Reference:

Bosi, F., Christy, A.G., and Hålenius, U. (2017): Crystal-chemical aspects of the roméite group, A2Sb2O6Y, of the pyrochlore supergroup. Mineral. Mag., 81, 1287–1302.
Courtin-Nomade, A., Rakotoarisoa, O., Bril, H., Grybosa, M., Forestier, L., Foucher, F., Kunz, M. (2011): Weathering of Sb-rich mining and smelting residues: Insight in solid speciation and soil bacteria toxicity. Chem. Erde, 72, 29–39.
Đorđević, T., Kolitsch, U., Serafimovski, T., Tasev, G., Tepe, N., Stöger-Pollach, Hofmann, T., Boev, B. (2019): Mineralogy and weathering of realgar-rich tailings at a former As-Sb-Cr mine at Lojane, North Macedonia. Can. Mineral., 57, 10–21.

886

Biorestoration Potential of Carbonatogenic Bacteria on Lithotypes: SEM and AFM characterization

Dr. Luca Buccini[1], Francesca Benedetti[2], Matilde Kratter[2], Francesco Mura[1,3], Anacleto Proietti[1], Pierfrancesco Atanasio[1], Angela Cirigliano[2], Marco Rossi[1,3], Teresa Rinaldi[1,2], Daniele Passeri[1,3]
[1]Department of Basic and Applied Sciences for Engineering (SBAI), La Sapienza University of Rome, Rome , Italy, [2]Department of Biology and Biotechnologies "Charles Darwin", Sapienza University of Rome, Rome, Italy, [3]CNIS-Center for Nanotechnology Applied to Industry of La Sapienza, La Sapienza University of Rome, Rome, Italy

Poster Group 2

Background incl. aims.
Microbially-induced calcium carbonate precipitation (MICCP), a bio-geochemical process, is a promising technology for eco-friendly applications particularly in the restoration of ornamental limestones.
This study explores the efficacy of the biorestoration treatment using Lysinbacillus fusiformis 3.20 strain as a carrier for the MICCP on three different lithotypes: calcarenite (MC), travertine (TR), and marble (MA). Despite sharing similar mineral compositions, these lithologies originate from different depositional settings, resulting in different petrophysical properties and microstructural features. To understand the biomineralization of the three different lithotypes the surface alterations and nanostructural changes were characterized by SEM (Scanning Electron Microscopy) and AFM (Atomic Force Microscopy).

Methods.
Small bricks of the three lithologies were treated spraying the bacterium culture twice a day for seven days at 28°C. Nanocaracterization of the surfaces of the three lithotypes was performed pre- and post-treatment using the Zeiss Auriga (SEM) operating at 1.5 keV and Bruker's Dimension Icon (AFM) using RTESPA-300 probes in tapping mode.

Results.
SEM micrographs revealed significant differences between the untreated and treated samples, particularly on the surfaces of the MC and TR stones. The treated samples showed the presence of calcified bacterial cells and newly formed crystals. In the MC samples, the crystals presented rhombohedral shapes, while the TR samples showed less homogenous aggregates. However, the treatment showed no significant effect on the MA samples, as no visible crystals or bacterial cells were observed after treatment. AFM analysis confirmed these results, showing the presence of bacteria and new crystals on the MC and TR samples post-treatment, with the bacterium being able to deposit calcium carbonate on the pore edges and covering the surfaces.

Conclusion.
The results obtained in controlled laboratory conditions emphasize that for the same treatment, the morphological variations of the bioprecipitation changes are strongly dependent on the lithology. Thus, for a future in situ application of this technique for stone conservation and restoration, the treatment will be optimized depending taking into account the differences of the lithologies.

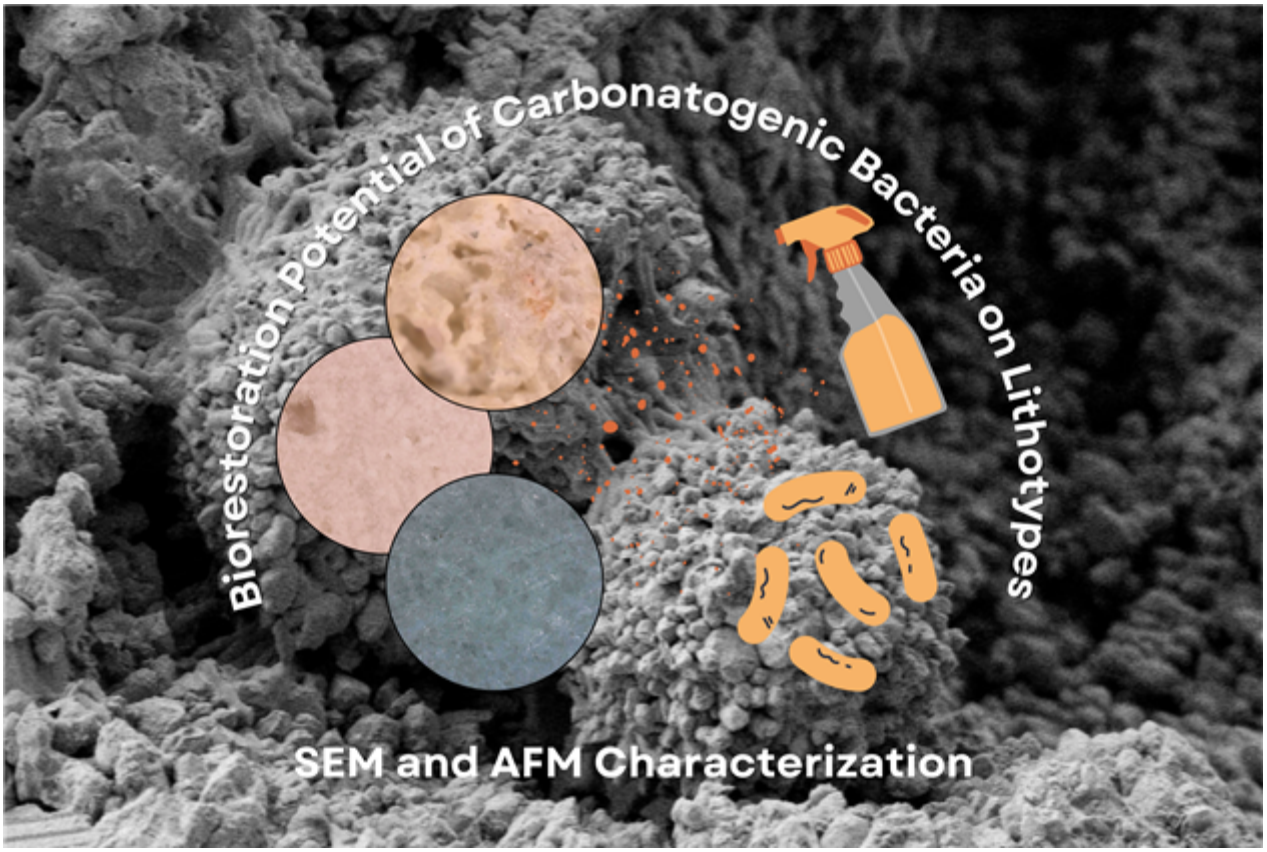

Keywords:

Biorestoration, SEM, AFM, biomineralization

Reference:

S. Ronca, F. Mura, M. Brandano, A. Cirigliano, F. Benedetti, A. Grottoli, M. Reverberi, D. F. Maras, R. Negri, E. Di Mauro, T. Rinaldi, Biogeosciences 2023, 20, 4135.
F. Benedetti, M. Kratter, P. Atanasio, F. Mura, M. Beccaccioli, J. Scifo, I. di Sarcina, M. C. Tomassetti, K. Schneider, M. Rossi, A. Cemmi, L. Nigro, T. Rinaldi, J. Cult. Herit. 2023, 64, 282.
P. Tiano, L. Biagiotti, G. Mastromei, J. Microbiol. Methods 1999, 36, 139.
L. Nigro, F. Mura, M. P. Toti, A. Cirigliano, T. Rinaldi, J. Cult. Herit. 2022, 57, 256.
F. Jroundi, M. Schiro, E. Ruiz-Agudo, K. Elert, I. Martín-Sánchez, M. T. González-Muñoz, C. Rodriguez-Navarro, Nat. Commun. 2017 81 2017, 8, 1.

1102

Room temperature viscoplastic response of amorphous olivine films revealed by ex/in-situ TEM nanomechanical testing

Dr Armand Béché[1]
[1]IMAP/LACaMi - UCLouvain, Louvain-La-Neuve, Belgium

Poster Group 2

Olivine is a silicate which controls the rheology of the Earth's mantle down to ca. 410 km depth. Recently, we have discovered a new deformation mechanism of olivine where grain boundary sliding involves amorphization of grain boundaries under high stresses and further plastic flow along this amorphous layer [1]. We are convinced that this mechanism has a fairly general application to hard materials under conditions of high stress. This idea has been previously advocated by Idrissi et al. [2]. In the present case of olivine, the implications are mainly in the lithosphere in a ductile brittle context and at the boundary between the lithosphere and the asthenosphere. This led us to characterize the mechanical properties of amorphous olivine, but this material is mostly available in the form of thin films. It is therefore necessary to employ nanomechanical techniques: nanoindentation, in-situ TEM deformation and Lab-on-Chip (Figure 1). These tests have in particular the capacity to extend the solicitations to very low deformation rates relevant in geodynamics. Advanced TEM characterizations have allowed to identify the underlying microscopic mechanisms either in-situ or in ex-situ deformed samples. These data will allow in the future to feed mesoscopic mechanical models of olivine-rich rocks of the upper mantle. We also observe a significant influence of the electron beam on the viscoplastic behaviour of amorphous olivine. Special attention was paid to elucidate the origin of such feature.

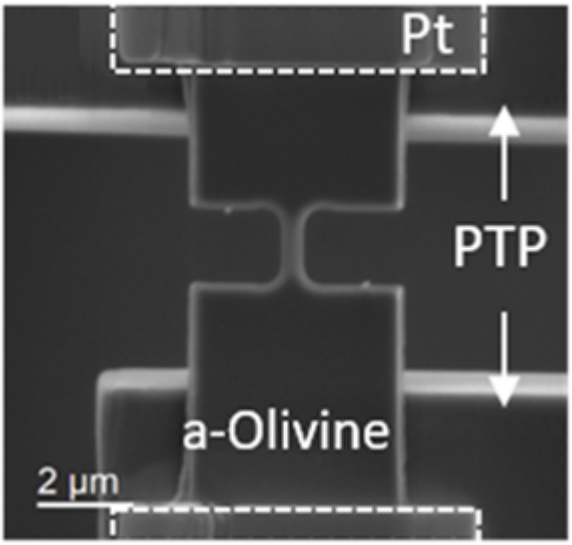

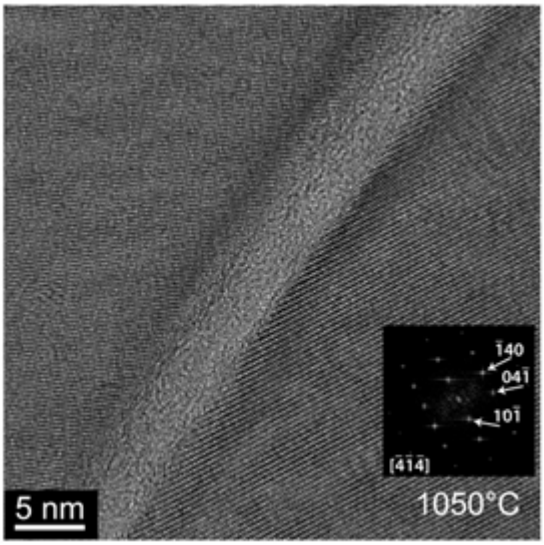

Keywords:

TEM, Olivine, Nano-mechanical testing, Lab-on-chip

Reference:

[1] V. Samae, P. Cordier, S. Demouchy, C. Bollinger, J. Gasc, S. Koizumi, A. Mussi, D. Schryvers & H. Idrissi, Nature, 2021, 591, 82.
[2] H. Idrissi, P. Carrez, P. Cordier, Current Opinion in Solid State and Materials Science, 2022, 26(1), 100976.

1124

SEM Automated Quantitative Mineralogy Method-development with Mineralogic: 200-nm-resolution Quantitative Assessment and Mineral-specific element mapping

Phd Nynke Keulen[1], MSc Sebastian N. Malkki[1], PhD Rikke Weibel[1], PhD Adam Garde[1]
[1]GEUS: Geological Survey of Denmark and Greenland, Copenhagen,

Poster Group 2

The study of fine-grained materials at the sub-micrometer scale with energy-dispersive X-ray spectroscopy (EDX) analysis using a scanning electron microscope (SEM) is often challenging. The primary electron beam's interaction-volume typically exceeds the grain size to be analyzed, resulting in mixed signals from individual grains. Consequently, EDX is rarely applied to such fine-grained materials. However, by employing a low primary beam acceleration voltage, a large aperture, and a dedicated mineral classification within the Zeiss Mineralogic software platform, mixed signals can be deconvoluted down to a spatial resolution of 200 nm [1]. This enables EDX and automated quantitative mineralogy (AQM) investigations of sub-micrometer-sized grains. Here, we would like to demonstrate reliable quantitative mineralogy on three case studies with geological samples with fine-grained material: 1) Fine-crushed fault gouge exhibiting a heterogeneous mineralogy, 2) fine needles in glass particles of a meteorite impact crater, and 3) rims in glauconite clasts affected by burial diagenesis.

Background

Automated Quantitative Mineralogy (AQM) has been applied since the early 1980s, applying technologies like QEMSCAN and the more recently TIMA-X. These techniques involve controlling the electron beam to scan the sample surface at a user-defined spatial resolution, capturing unquantified energy-dispersive spectroscopy (EDX) spectra. These unprocessed spectra are then matched to a reference library of known EDX spectra to identify minerals. This approach is very fast, however it provides only a rough assessment of mineralogy when elemental concentrations exceed ca. 10 wt%.

Method

The introduction of ZEISS' Mineralogic software advance AQM capabilities by integrating matrix corrections, and peak deconvolution in EDX spectra for each analysis point rather than matching spectra. Minerals are classified based on stoichiometry values. Importantly, the software retains the chemistry information for each pixel, allowing reinterpretation of mineralogy after analysis. Samples were polished and coated with carbon and examined using a Zeiss SIGMA 300VP SEM equipped with two Bruker XFlash 6|30 EDX detectors (129-eV energy resolution) and the Zeiss Mineralogic AQM mineralogy software platform. A specific region of interest was imaged to create a high-resolution back-scattered electron contrast mosaic [2]. Additionally, a 200-nm step-size AQM analysis was performed using Mineralogic, resulting in a detailed mineral map.

X-rays are generated from an interaction volume, which size depends on the primary energy of the beam and the mean atomic number of the sample. The interaction volumes for geological samples (silicates) typically ranges from 2 to 5 µm when using a 20-kV primary electron beam. For minerals with finer grain sizes however, accurate chemical analysis and mineral classification based solely on EDX spectra is therefore challenging as the resulting spectrum will consist of a compositional "mixing" of multiple grains. To address this, the interaction volume was reduced by setting the acceleration volume of the primary beam to 10 kV, while applying a 60-µm aperture providing a 1.8-nA beam current, to minimizing the interaction volume and therefore the amount of signal mixing, while keeping a high-enough signal to resolve all relevant elements in silicates. Despite this

reduction, Monte Carlo simulations indicated that minerals with the lowest average atomic number (Z) still yielded an interaction volume diameter of approximately 1 µm, while high-Z phases reached down to 400 nm. The 200-nm EDX pixel size allowed for oversampling and captured a significant volume of mixed pixel signatures. But the integration of fully quantitative energy-dispersive X-ray spectroscopy (EDX) classifications within the Zeiss Mineralogic software allows for precise analysis at the pixel level [2]. By quantifying the weight percent contribution of elements on a per-pixel basis, the software discriminates minerals effectively, even when dealing a certain amount of contamination resulting from mixed signals. Even for minerals with a low atomic number (Z), where the interaction volume is relatively high, Monte Carlo simulations demonstrate that a significant portion of chemical information originates from the localized area where the electron beam strikes the sample. By leveraging this insight, the software accurately translates mixed signals into mineral classifications, ensuring correct identification and analysis of these particles [1].

To perform mineral-specific element mapping, the technique above is further adapted in the ZEISS Mineralogic software platform to be able to visualise the element distribution in selected minerals, while masking out the other minerals simultaneously [3].

Results
In the presentation will be shown that polymineralic fault gouge down to 200 nm in diameter can be differentiated, classified from the data for that pixel, and its grain size distribution can be assessed [1]. Micrometer and submicrometer scale features in grains collected from the Hiawatha impact crater reveal the history of the area during and after the impact. Acicular orthopyroxene microlites, with a 1-2 µm width, were crystallized from melts above the solidus under different degrees of undercooling. Emulsion microstructures with siliceous melt droplets in an iron-rich melt phase show internal zonation at µm-scale, interpreted as incomplete mixing between two shock melts with different compositions forming equant, micrometer-sized microlites. Felsic melt grains contains abundant, closely packed microspherulites of 1-3 µm mordenite, giving evidence for a hydration event [4]. Rimmed glauconitic clasts reveal different trends during burial of glauconitic sandstone: the composition of the glauconite grains changes with depth, they become on average more K-rich and Fe-poor, with exception those being chlorite-replaced. This is an alteration effect, depending on temperature, distance to embedding mudstones and/or fluid composition, and the illitization of glauconitic clasts, at increasing depth. Nearly all glauconitic clasts have rims richer in Al and poorer in Fe and K, related to late diagenetic alteration, either resulting from the reaction to smectite or due to interaction with brine or hydrocarbons [3,5].

Conclusions
The ability to quantify the EDX spectrum at each analyzed point into its primary chemical components, and the use of in-built matrix corrections and peak deconvolutions, provide a robust analytical framework to provide high-quality quantitative chemical and mineralogical data that open up for a range of new applications in AQM.

Keywords:

Automated-Quantitative-Mineralogy
high-resolution EDS
Mineral-specific element-mapping

Reference:

1. Graham, S.; Keulen, N. Nanoscale Automated Quantitative Mineralogy: A 200-nm Quantitative Mineralogy Assessment of Fine-grained Fault Gouge Using Mineralogic. Minerals 2019, 9, 665; doi:10.3390/min9110665.

2. Keulen, N.; Malkki, S.N.; Graham, S. Automated quantitative mineralogy applied to metamorphic rocks. Minerals 2020, 10, 47; doi:10.3390/min10010047.
3. Keulen, N., Weibel, R. & Malkki, S.N. 2022: Mineral-specific Quantitative Element Mapping Applied to Visualization of Geochemical Variation in Glauconitic Clasts. Frontiers in Earth Sciences, 9pp, doi: 10.3389/feart.2022.788781
4. Garde, A., Keulen, N., Waight, T. 2022: Microporphyritic and microspherulitic melt grains, Hiawatha crater, Northwest Greenland: Implications for post-impact cooling rates, hydration, and the cratering environment. The Geological Society of America, 22p. doi: 110.1130./B36058.1
5. Weibel, R., Keulen, N., Hillier, S., Friis, H., Petersen, H.I., Olivarius, M., Malkki, S.N., Stokkendal, J., Schovsbo, N.H. 2023: Reactivity of glauconitic clasts during burial diagenesis. Sedimentary Geology 458: 106519. https://doi.org/10.1016/j.sedgeo.2023.106519

1146

ESEM technique for monitoring the geo-polymerization mechanism of the wet ash-cement mixture

Phd Bogdan Stefan Vasile[1], Dr. Iulian Boerasu[3], Dr. Adrian-Vasile Surdu[2], Dr. Adrian Ionut Nicoara[2]
[1]Research Center for Advanced Materials, Products and Processes, National University of Science and Technology POLITEHNICA Bucharest, 060042 Bucharest, Romania, Bucharest, Romania, [2]Department of Science and Engineering of Oxide Materials and Nanomaterials, Faculty of Applied Chemistry and Materials Science, University Politehnica of Bucharest, 011061 Bucharest, Romania, Bucharest, Romania, [3]National Research Center for Micro and Nanomaterials, Faculty of Applied Chemistry and Materials Science, University Politehnica of Bucharest, 060042 Bucharest, Romania, Bucharest, Romania

Poster Group 2

Background
Portland cement is one of the most important material of any country infrastructure development. Due to the massive global production and consumption of Portland cement, the cement industry is responsible for almost 10% of the world's carbon dioxide emissions associated with anthropogenic activities [1] and consumes about 3% of the world's energy [2]. Recent studies have demonstrated that fly-ash (FA) can be used as a mineral admixture in the cement industry to reduce the consumption of the most common calcareous raw materials [3].
Herein, we report on the benefits of the ESEM (Environmental Scanning Electron Microscopy) technique to expand the in situ knowledge of the geo-polymerization mechanism of the FA-cement mixture in the wet state. Moreover, X-ray diffraction (XRD) results about the phase composition and crystallinity of the initial ash, as well as in-situ evaluation for hydration of cement pastes, are reported.

Methods
Ash and slag from the Turceni thermal power plant deposit were used as supplementary cementitious materials (SCMs) to replace ordinary Portland cement.
The microstructure of the cement pastes and the in-situ reaction products formed during the first minutes to hours were studied using the Versa 3D Scanning Electron Microscope, which allows the adjustment of pressure, temperature, and humidity. Imaging was performed at a temperature of 2 0C and relative humidity of 90%, with a beam voltage of 30 kV, at a working distance of 9 mm. Morphology changes during hydration of cement pastes were in-situ ESEM monitored under a relative humidity of 90% and at a temperature of 2 0C. According to the pressure-humidity-temperature diagram of the liquid-vapor phase diagram for water, the expected pressure in the working chamber was estimated to be ~640 Pa. It is worth mentioning that the is situ ESEM dynamic experiments were performed on uncoated fresh wet cement mixture pastes. Each sample was monitored for a period of 3 to 6 h (depending on the specificity of the observed morphological changes) and the images were acquired every 10 min at magnifications of ×5,000 and ×10,000. Scanning electron microscopy (SEM) analysis of the ash powder and cement pastes after several days of curing was performed using an FEI Inspect F50 microscope coupled with an energy dispersive spectrometer (EDS) (ThermoFisher, Eindhoven, The Netherlands).
The phase composition and crystallinity of the initial ash, as well as in-situ evaluation for hydration of cement pastes, were studied by X-ray diffraction (XRD) using PANalytical Empyrean equipment. The equipment was used in transmission geometry and was equipped with a hybrid monochromator and a 1/20 divergent slit on the incident beam side and a programmable anti-scattering slit mounted on the PIXCel3D detector on the diffracted beam side. The sample was investigated in the range of 4–480 2θ angle. Measurements were performed every 15 min for 24 h. Reduction of X-ray diffraction

data and full pattern fitting by the Rietveld method were performed using HighScorePlus 3.0.e software (PANalytical, Almelo, The Netherlands).

Results

The morphologies for the reference sample C0 (100% cement) and the sample C45 (55% cement and 45% ash) are shown in Figure 1. The legends show the time of acquisition, with the first image taken immediately after the “dead” time limit, called t0. In the micrographs in Figure 1a) of hydrated cement paste (sample C0) it can be seen the evolution of the first hydration products cement, with the formation of acicular structures of ettringite and CSH/CASH (calcium/aluminium silicate hydrates) [4, 5]. Smaller particles are more reactive compared to larger ones. The hydration products tended to crystallize into cracks and pore spaces. A significant amount of cement hydration reactions appeared to have occurred during the “dead” period. The soft and fragile bride’s veil morphology of CSH appeared to have emerged from all surfaces. As revealed by Figure 1b), the addition of high ash content (sample C45) induced a delay in the hydration reactions, with the formation of prismatic sheet structures over time. The hydration products appeared even more crystalline. The usual amorphous CSH veil structure appeared at later stages (420 min) of hydration. As the paste hydrates over time, the hydrogel resulting from the partial hydration of mineralogical compounds such as dicalcium silicate, tricalcium silicate, and tricalcium aluminate, covered the spaces between the particles of the specimen. At this highest loading content of ash into cement pastes (sample C45), the formed crystals appeared to have better-defined edges. Ca(OH)2 platelet structures could be captured after the “dead” time. The gel-like hydrosilicates covered the ash particles very well, and the needle structures responsible for the subsequent mechanical strengths of the binder material can be visualized in the advanced moments of hydration (t0 + 20’, t0 + 420’).

The XRD patterns obtained for the C0 and C45 sample, at the initial time point and after different time intervals from 15 min to 24 h, are depicted in Figure 2. According to the recorded spectrum, the intensity of the peaks decreases with time, as a consequence of a decreasing in the degree of crystallinity (anhydrous phase content). As seen in Figure 2, the cement substitution with FA in a proportion of 45% did not drastically alter the phase evolution during hydration.

Conclusions

The herein reported in-situ ESEM and in-situ XRD has revealed new insides about the geo-polymerization mechanism of the FA-cement mixture in the wet state. The addition of ash in different proportions affects the hydration kinetics in the sense that some hydration reactions of the mineralogical binders are delayed with increasing ash content whereas Ca-initiated ones are accelerated.

Sustainability through the reuse of accessible economic and social resources is a way to achieve environmental balance while ensuring long-term development. The obtained results have confirmed the ash from Turceni thermal power plant features as SCM material to replace ordinary Portland cement.

Keywords:

ESEM, IN-Situ Hydration

Reference:

[1] Snellings, R.; Horckmans, L.; Van Bunderen, C.; Vandewalle, L.; Cizer, Ö. Flash-calcined dredging sediment blended cements: Effect on cement hydration and properties. Mater. Struct. 2017, 50, 241.
[2] Sivakrishna, A.; Adesina, A.; Awoyera, P.; Kumar, K.R. Green concrete: A review of recent developments. Mater. Today Proc. 2020, 27, 54–58.
[3] Rastogi, A.; Paul, V.K. A critical review of the potential for fly ash utilisation in construction-specific applications in India. Environ. Res. Eng. Manag. 2020, 76, 65–75.